

Multiscale mixed finite elements

Fredrik Hellman¹, Patrick Henning², Axel Målqvist³

June 21, 2016

Abstract

In this work, we propose a mixed finite element method for solving elliptic multiscale problems based on a localized orthogonal decomposition (LOD) of Raviart–Thomas finite element spaces. It requires to solve local problems in small patches around the elements of a coarse grid. These computations can be perfectly parallelized and are cheap to perform. Using the results of these patch problems, we construct a low dimensional multiscale mixed finite element space with very high approximation properties. This space can be used for solving the original saddle point problem in an efficient way. We prove convergence of our approach, independent of structural assumptions or scale separation. Finally, we demonstrate the applicability of our method by presenting a variety of numerical experiments, including a comparison with an MsFEM approach.

Keywords mixed finite elements, multiscale, numerical homogenization, Raviart–Thomas spaces, upscaling

AMS subject classifications 35J15, 35M10, 65N12, 65N30, 76S05

1 Introduction

In this work we study the mixed formulation of Poisson’s equation with a multiscale diffusion coefficient, i.e. where the diffusion coefficient is highly varying on a continuum of different scales. For such coefficients, the solution is typically also highly varying and standard Galerkin methods fail to converge to the correct solution, unless the features on the finest scale are resolved by the underlying computational mesh. A classical application is the flow in a porous medium, modeled by Darcy’s law. In this case, the multiscale coefficient describes a permeability field, which is heterogeneous, rapidly varying and has high contrast. Classical discretizations that involve the full fine scale often lead to a vast number of degrees of freedom, which limits the performance and feasibility of corresponding computations. In this paper, we address this kind of problems in the context of mixed finite elements.

We will interpret the mixed formulation of Poisson’s equation in a Darcy flow setting, referring to the vector component as flux, and the scalar component as pressure.

¹Department of Information Technology, Uppsala University, Box 337, SE-751 05 Uppsala, Sweden. Supported by Centre for Interdisciplinary Mathematics (CIM), Uppsala University.

²Department of Mathematics, KTH Royal Institute of Technology, SE-100 44 Stockholm, Sweden.

³Department of Mathematical Sciences, Chalmers University of Technology and University of Gothenburg SE-412 96 Göteborg, Sweden. Supported by the Swedish Research Council.

In Darcy flow applications the flux solution is of particular interest since it tells us how a fluid is transported through the medium. It is desirable and common to use flux conservative discretization schemes. The proposed method is based on the Raviart–Thomas finite element [31] which is locally flux conservative. Concerning the mixed formulation of Poisson’s equation, corresponding multiscale methods were for instance proposed in [1, 5, 6, 9]. These methods are based on the Raviart–Thomas finite element and fit into the framework of the Multiscale Finite Element Method (MsFEM, cf. [19]). Another family of multiscale methods is derived from the framework of the Variational Multiscale Method (VMS) [20, 21, 22, 24, 29]. Multiscale methods for mixed finite elements based on VMS are proposed and studied in [4, 25, 28]. Inspired by the results presented in [28], a new multiscale framework arose [26]. We refer to this framework as Localized Orthogonal Decomposition (LOD). It is based on the idea that a finite element space is decomposed into a low dimensional space that incorporates multiscale features and a high dimensional remainder space which is given as the kernel of an interpolation or quasi-interpolation operator. The multiscale space can be used for Galerkin-approximations and allows for cheap computations. Various realizations have been proposed so far. For corresponding formulations and rigorous convergence results for elliptic multiscale problems, we refer to [2, 14, 15, 18, 26] for Galerkin finite element methods, to [13, 14] for discontinuous Galerkin methods and to [17] for Galerkin Partition of Unity methods. Among the various applications we refer to the realizations for eigenvalue problems [27], for semilinear equations [16], for the wave equation [3] and for the Helmholtz equation [30].

In this paper we introduce a two level discretization of the mixed problem, that is we work with two meshes: A fine mesh (mesh size h) which resolves all the fine scale features in the solution and a coarse mesh (mesh size H) which is of computationally feasible size. This gives us a fine and a coarse Raviart–Thomas function space for the flux. We denote them respectively by V_h (high dimensional) and V_H (low dimensional). The kernel of the (standard) nodal Raviart–Thomas interpolation operator Π_H onto V_H is the detail space V_h^f . This space can be interpreted as all fine scale features that can not be captured in the coarse space V_H . A low dimensional ideal multiscale space is constructed as the orthogonal complement to the divergence free fluxes in V_h^f . We prove that this space has good approximation properties in the sense that the energy norm of the error converges with H without pre-asymptotic effects due to the multiscale features. However, the basis functions of the ideal multiscale space have global support and are expensive to compute. We show exponential decay of these basis functions allowing them to be truncated to localized patches with a preserved order of accuracy for the convergence. The resulting space is called the localized multiscale space. The problems that are associated with the localized basis functions have a small number of degrees of freedom and can be solved in parallel with reduced computational cost and memory requirement. Once computed, the low dimensional localized multiscale space can be reused in a nonlinear or time iterative scheme.

We prove inf-sup stability and a priori error estimates (of linear order in H) for both the ideal and the localized method. The local L^2 -instability of the nodal Raviart–Thomas interpolation operator leads to instabilities as h decreases for the localized method. We show that these instabilities can be compensated by increasing the patch size or using Clément-type interpolators instead. In the numerical examples we verify that the localized method has the theoretically derived order of accuracy. We confirm our theoretical

findings by performing experiments on the unit square and an L-shaped domain, as well as using a diffusion coefficient with high contrast noise and channel structures. The proposed method is also compared numerically with results from an MsFEM-based approach using a permeability field from the SPE10 benchmark problem.

2 Preliminaries

We consider a bounded Lipschitz domain $\Omega \subset \mathbb{R}^d$ (dimension $d = 2$ or 3) with a piecewise polygonal boundary $\partial\Omega$ and let \mathbf{n} denote the outgoing normal vector of $\partial\Omega$. For any subdomain $\omega \subseteq \Omega$, we shall use standard notation for Lebesgue and Sobolev spaces, i.e. for $r \in [1, \infty]$, $L^r(\omega)$ consists of measurable functions with bounded L^r -norm and the space $H^1(\omega)$ consists of L^2 -bounded weakly differentiable functions with L^2 -bounded partial derivatives. The full norm on $H^1(\omega)$ shall be denoted by $\|\cdot\|_{H^1(\omega)}$, whereas the semi-norm is denoted by $|\cdot|_{H^1(\omega)} := \|\nabla \cdot\|_{L^2(\omega)}$.

For scalar functions p and q we denote by $(p, q)_\omega := \int_\omega pq$ the L^2 -scalar product on ω . When $\omega = \Omega$, we omit the subscript, i.e. $(p, q) := (p, q)_\Omega$. For d -dimensional vector valued functions \mathbf{u} and \mathbf{v} , we define $(\mathbf{u}, \mathbf{v})_\omega := \int_\omega \mathbf{u} \cdot \mathbf{v}$ with $(\mathbf{u}, \mathbf{v}) = (\mathbf{u}, \mathbf{v})_\Omega$. Observe that we use the same notation for norms and scalar products in L^2 without distinguishing between scalar and vector valued functions. This is purely for simplicity, since the appropriate definition is always clear from the context. We use, however, bold face letters for vector valued quantities.

In the following, we define the Sobolev space of functions with L^2 -bounded weak divergence by $H(\text{div}, \omega) := \{\mathbf{v} \in [L^2(\omega)]^d : \nabla \cdot \mathbf{v} \in L^2(\omega)\}$. We equip this space with the usual norm $\|\cdot\|_{H(\text{div}, \omega)}$, where $\|\mathbf{v}\|_{H(\text{div}, \omega)}^2 := \|\nabla \cdot \mathbf{v}\|_{L^2(\omega)}^2 + \|\mathbf{v}\|_{L^2(\omega)}^2$. Additionally, for $\omega = \Omega$, we introduce the subspace $H_0(\text{div}, \Omega) := \{\mathbf{v} \in H(\text{div}, \Omega) : \mathbf{v} \cdot \mathbf{n}|_{\partial\Omega} = 0\}$ of functions with zero flux on the boundary, where $\mathbf{v} \cdot \mathbf{n}|_{\partial\Omega}$ should be interpreted in the sense of traces. We denote by $L^2(\Omega)/\mathbb{R} := \{q \in L^2(\Omega) : \int_\Omega q = 0\}$ the quotient space of $L^2(\Omega)$ by \mathbb{R} . The continuous dual space of a Banach space X is denoted by X' .

2.1 Continuous problem

With these definitions we are ready to state the continuous problem, which is Poisson's equation in mixed form with Neumann boundary conditions on the full boundary.

Definition 1 (Continuous problem). *Find $\mathbf{u} \in V := H_0(\text{div}, \Omega)$, $p \in Q := L^2(\Omega)/\mathbb{R}$ such that*

$$\begin{aligned} (\mathbf{A}^{-1}\mathbf{u}, \mathbf{v}) + (\nabla \cdot \mathbf{v}, p) &= 0, \\ (\nabla \cdot \mathbf{u}, q) &= -(f, q), \end{aligned} \tag{1}$$

for all $\mathbf{v} \in V$, $q \in Q$.

We pose the following assumptions on the coefficient and data.

Assumption A (Assumptions on coefficients, data and domain).

(A1) $\mathbf{A} \in [L^\infty(\Omega)]^{d \times d}$ is a diffusion coefficient, possibly with rapid fine scale variations. Its value is an almost everywhere symmetric matrix and bounded in the sense that

there exist real numbers α and β such that for almost every x and any $\mathbf{v} \in \mathbb{R}^d/\{0\}$

$$0 < \alpha \leq \frac{(\mathbf{A}(x)^{-1}\mathbf{v}) \cdot \mathbf{v}}{\mathbf{v} \cdot \mathbf{v}} \leq \beta < \infty.$$

(A2) $f \in L^2(\Omega)$ is a source function that fulfills the compatibility condition $\int_{\Omega} f = 0$.

(A3) The domain Ω is a bounded Lipschitz domain with polygonal (or polyhedral) boundary.

We introduce the following bilinear forms and norms. Let

$$a(\mathbf{u}, \mathbf{v}) := (\mathbf{A}^{-1}\mathbf{u}, \mathbf{v}) \quad \text{and} \quad b(\mathbf{v}, q) := (\nabla \cdot \mathbf{v}, q)$$

and, further,

$$\|\mathbf{v}\|_V := \|\mathbf{v}\|_{H(\text{div}, \Omega)} \quad \text{and} \quad \|q\|_Q := \|q\|_{L^2(\Omega)}.$$

The energy norm is defined as the following weighted flux L^2 -norm,

$$\|\mathbf{v}\|^2 := \|\mathbf{A}^{-1/2}\mathbf{v}\|_{L^2(\Omega)}^2 = a(\mathbf{v}, \mathbf{v})$$

The energy norm can be subscripted with a subdomain $\omega \subseteq \Omega$, for example $\|\cdot\|_{\omega}^2$, to indicate that the integral is taken only over that subdomain.

The following lemma gives the conditions for existence and uniqueness of a solution to the mixed formulation in (1) for subspaces $\mathcal{V} \subseteq V$ and $\mathcal{Q} \subseteq Q$. This lemma is useful for establishing existence and uniqueness for all discretizations presented in this paper, since all presented discretizations are conforming.

Lemma 2 (Existence and uniqueness of solution to mixed formulation). *Let $\mathcal{V} \subseteq V$ and $\mathcal{Q} \subseteq Q$. Denote by $\mathcal{K} = \{\mathbf{v} \in \mathcal{V} : b(\mathbf{v}, q) = 0 \ \forall q \in \mathcal{Q}\}$. If $a(\cdot, \cdot)$ is coercive on \mathcal{K} with constant $\tilde{\alpha} > 0$, i.e. $a(\mathbf{v}, \mathbf{v}) \geq \tilde{\alpha}\|\mathbf{v}\|_V^2$ for $\mathbf{v} \in \mathcal{K}$, and bounded with constant $\tilde{\beta} > 0$, i.e. $|a(\mathbf{v}, \mathbf{w})| \leq \tilde{\beta}\|\mathbf{v}\|_V\|\mathbf{w}\|_V$ for all $\mathbf{v}, \mathbf{w} \in \mathcal{V}$, and additionally $b(\cdot, \cdot)$ is inf-sup stable with constant $\tilde{\gamma} > 0$, i.e.*

$$\inf_{q \in \mathcal{Q}} \sup_{\mathbf{v} \in \mathcal{V}} \frac{b(\mathbf{v}, q)}{\|\mathbf{v}\|_V \|q\|_Q} \geq \tilde{\gamma},$$

then the problem $a(\mathbf{u}, \mathbf{v}) + b(\mathbf{v}, p) - b(\mathbf{u}, q) = (f, q)$ for all $(\mathbf{v}, q) \in \mathcal{V} \times \mathcal{Q}$ has a unique solution $(\mathbf{u}, p) \in \mathcal{V} \times \mathcal{Q}$ bounded by

$$\|\mathbf{u}\|_V \leq \frac{2\tilde{\beta}^{1/2}}{\tilde{\alpha}^{1/2}\tilde{\gamma}} \|f\|_{L^2(\Omega)} \quad \text{and} \quad \|p\|_Q \leq \frac{\tilde{\beta}}{\tilde{\gamma}^2} \|f\|_{L^2(\Omega)}.$$

Proof. See e.g. [8, Theorem 4.2.3]. □

Under Assumptions (A1)–(A3), the conditions for Lemma 2 are satisfied for $\mathcal{V} = V$ and $\mathcal{Q} = Q$ with $\tilde{\alpha} = \alpha$, $\tilde{\beta} = \beta$ and $\tilde{\gamma}$ being a constant that depends only on the computational domain. The lemma then yields a unique solution to the continuous problem (1).

2.2 Discretization with the Raviart–Thomas element

Regarding the discretization, we introduce two conforming families of simplicial (i.e. triangular or tetrahedral) meshes $\{\mathcal{T}_h\}$ and $\{\mathcal{T}_H\}$ of Ω where h and H are the maximum element diameters. Throughout the paper we refer to \mathcal{T}_h as the fine mesh and to \mathcal{T}_H as the coarse mesh. Hence, we indirectly assume $h \ll H$. We pose the following assumptions on the meshes.

Assumption B (Assumptions on meshes).

- (B1) *The fine mesh \mathcal{T}_h is the result of one or more conforming (but possibly non-uniform) refinements of the coarse mesh \mathcal{T}_H such that $\mathcal{T}_h \cap \mathcal{T}_H = \emptyset$.*
- (B2) *Both meshes \mathcal{T}_h and \mathcal{T}_H are shape regular. In particular the positive shape regularity constant ρ for the coarse mesh \mathcal{T}_H will be referred to below and is defined as $\rho = \min_{T \in \mathcal{T}_H} \frac{\text{diam } B_T}{\text{diam } T}$ where B_T is the largest ball contained in the element $T \in \mathcal{T}_H$.*
- (B3) *The coarse family of meshes $\{\mathcal{T}_H\}$ is quasi-uniform, whereas $\{\mathcal{T}_h\}$ could be obtained from an arbitrary adaptive refinement.*

Remark 3 (Quadrilateral or hexahedral elements). *Affine quadrilateral (or hexahedral) elements can also be used. However, the definition of the Raviart–Thomas element presented below in this paper is based on triangular (or tetrahedral) meshes.*

We denote by t and T an element of \mathcal{T}_h or \mathcal{T}_H , respectively. Similarly e and E denote an edge (for $d = 2$) or a face (for $d = 3$) of the elements of \mathcal{T}_h and \mathcal{T}_H . Further, \mathbf{n}_e (respectively \mathbf{n}_E) is the outward normal vector of an edge (or face) e (respectively E). We continue this section by discussing finite element discretizations using the two meshes.

We denote all polynomials of degree $\leq k$ on a subdomain ω by $\mathbb{P}^k(\omega)$ and a d -dimensional vector of such polynomials by $[\mathbb{P}^k(\omega)]^d$. We introduce the $H_0(\text{div}, \Omega)$ -conforming lowest (zeroth) order Raviart–Thomas finite element. For each fine element $t \in \mathcal{T}_h$ and coarse element $T \in \mathcal{T}_H$, the spaces of Raviart–Thomas shape functions are given by

$$\begin{aligned} \mathcal{RT}_h(t) &= \{\mathbf{v}|_t = [\mathbb{P}^0(t)]^d + x\mathbb{P}^0(t)\} \text{ and} \\ \mathcal{RT}_H(T) &= \{\mathbf{v}|_T = [\mathbb{P}^0(T)]^d + x\mathbb{P}^0(T)\}, \end{aligned}$$

respectively, where $x = (x_1, \dots, x_d)$ is the space coordinate vector. The Raviart–Thomas finite element spaces on \mathcal{T}_h and \mathcal{T}_H are then defined as

$$\begin{aligned} V_h &= \{\mathbf{v} \in H_0(\text{div}, \Omega) : \mathbf{v}|_t \in \mathcal{RT}_h(t) \quad \forall t \in \mathcal{T}_h\} \text{ and} \\ V_H &= \{\mathbf{v} \in H_0(\text{div}, \Omega) : \mathbf{v}|_T \in \mathcal{RT}_H(T) \quad \forall T \in \mathcal{T}_H\}. \end{aligned}$$

The degrees of freedom (in the coarse and fine Raviart–Thomas spaces) are given by the averages of the normal fluxes over the edges (respectively faces for $d = 3$). We denote the degrees of freedom by

$$N_e(\mathbf{v}) := \frac{1}{|e|} \int_e \mathbf{v} \cdot \mathbf{n}_e \quad \text{and} \quad N_E(\mathbf{v}) := \frac{1}{|E|} \int_E \mathbf{v} \cdot \mathbf{n}_E$$

for the fine and coarse discretization, respectively. The direction of the normal \mathbf{n}_e (respectively \mathbf{n}_E) can be fixed arbitrarily for each edge (respectively face). Here, N_e and N_E are

bounded linear functionals on the space $W := H_0(\operatorname{div}, \Omega) \cap L^s(\Omega)$, for some $s > 2$. Note, that the additional regularity (i.e. $L^s(\Omega)$ for $s > 2$) is necessary for the edge integrals to be well-defined (cf. [8]). We introduce the (standard) nodal Raviart–Thomas interpolation operators $\Pi_h : W \rightarrow V_h$ and $\Pi_H : W \rightarrow V_H$ by fixing the degrees of freedom in the natural way, i.e. Π_h and Π_H are defined such that

$$N_e(\Pi_h \mathbf{v}) = N_e(\mathbf{v}) \quad \text{and} \quad N_E(\Pi_H \mathbf{v}) = N_E(\mathbf{v}).$$

Additionally, we let $Q_H \subset Q_h \subset Q$ be the space of all piecewise constant functions on \mathcal{T}_H and \mathcal{T}_h with zero mean. We denote by P_h and P_H the L^2 -projections onto Q_h and Q_H , respectively. Using the fine spaces, we define the fine scale discretization of (1), which will be referred to as the reference problem.

Definition 4 (Reference problem). *Find $\mathbf{u}_h \in V_h$ and $p_h \in Q_h$, such that*

$$\begin{aligned} a(\mathbf{u}_h, \mathbf{v}_h) + b(\mathbf{v}_h, p_h) &= 0, \\ b(\mathbf{u}_h, q_h) &= -(f, q_h), \end{aligned} \tag{2}$$

for all $\mathbf{v}_h \in V_h$ and $q_h \in Q_h$.

A similar problem can be stated with the coarse spaces V_H and Q_H with flux solution \mathbf{u}_H . The remainder of this section treats only the fine discretization. However, all results hold also for the coarse discretization.

We denote the space of divergence free functions on the fine grid by

$$K_h := \{\mathbf{v} \in V_h : \nabla \cdot \mathbf{v} = 0\}. \tag{3}$$

Remark 5 (Kernel of divergence operator). *A natural definition of K_h for our purposes is $K_h = \{\mathbf{v} \in V_h : (\nabla \cdot \mathbf{v}, q_h) = 0 \ \forall q_h \in Q_h\}$. However, since we have $\nabla \cdot \mathbf{v} \in Q_h$ for all $\mathbf{v} \in V_h$ (due to the definition of the Raviart–Thomas element), we can characterize K_h equivalently as done in (3).*

To establish existence and uniqueness of a solution to the reference problem, we use that Π_h is divergence compatible, i.e. we have the commuting property $\nabla \cdot \Pi_h \mathbf{v} = P_h \nabla \cdot \mathbf{v}$ for $\mathbf{v} \in W$, and that Π_h is bounded on W (but not on V !), i.e. there exists a generic h -independent constant C_W such that $\|\Pi_h \mathbf{v}\|_V \leq C_W \|\mathbf{v}\|_W$ for $\mathbf{v} \in W$. Using this, the inf-sup stability of $b(\cdot, \cdot)$ with respect to V_h and Q_h follows: For $q \in Q_h$,

$$\begin{aligned} \sup_{\mathbf{v} \in V_h} \frac{b(\mathbf{v}, q)}{\|\mathbf{v}\|_V} &= \sup_{\mathbf{v} \in W} \frac{(\nabla \cdot \Pi_h \mathbf{v}, q)}{\|\Pi_h \mathbf{v}\|_V} \geq \sup_{\mathbf{v} \in W} \frac{(\nabla \cdot \mathbf{v}, q)}{C_W \|\mathbf{v}\|_W} \\ &\geq \frac{(\nabla \cdot \mathbf{w}, q)}{C_W \|\mathbf{w}\|_W} \geq \frac{(q, q)}{C_W C_\Omega \|q\|_{L^2(\Omega)}} = C_W^{-1} C_\Omega^{-1} \|q\|_{L^2(\Omega)}, \end{aligned} \tag{4}$$

where $\mathbf{w} \in W$ is chosen such that $\nabla \cdot \mathbf{w} = q$ and $\|\mathbf{w}\|_W \leq C_\Omega \|q\|_{L^2(\Omega)}$. This is possible by letting $\mathbf{w} = \nabla \phi$ for a solution ϕ to $\Delta \phi = q$ in Ω with homogeneous Neumann boundary conditions. Now, applying Lemma 2 with $\mathcal{V} = V_h$, $\mathcal{Q} = Q_h$, $\mathcal{K} = K_h$, we can derive the constants $\tilde{\alpha} = \alpha$, $\tilde{\beta} = \beta$ and $\tilde{\gamma} = \gamma := C_W^{-1} C_\Omega^{-1}$ and establish existence and uniqueness of a solution to the reference problem (2). Note that the inf-sup stability constant γ is independent of h and hence also holds for the pair of spaces V_H and Q_H .

In the following, we are mainly interested in approximating the flux component \mathbf{u}_h of the solution. We treat \mathbf{u}_h as a reliable reference to the exact solution. Note that the L^2 -norm of the divergence error is controlled by the data

$$\|\nabla \cdot \mathbf{u} - \nabla \cdot \mathbf{u}_h\|_{L^2(\Omega)} \leq \|f - P_h f\|_{L^2(\Omega)}.$$

For the energy norm of the flux error, we have the following error estimate in the energy norm for the lowest order Raviart–Thomas element:

$$\|\mathbf{u} - \mathbf{u}_h\| \leq Ch |\mathbf{u}|_{H^1(\Omega)},$$

where C is independent of h . For a problem with a coefficient \mathbf{A} that has fast variations at a scale of size ϵ , we have in general that $|\mathbf{u}|_{H^1(\Omega)} \approx \epsilon^{-1}$. Hence, we require $h \ll \epsilon$ before we can observe the linear convergence in h numerically. We call the regime with $h \geq \epsilon$ a pre-asymptotic regime. The goal of this work is the construction of a discrete space which does not suffer from such pre-asymptotic effects triggered by \mathbf{A} . In the following, we assume that the fine mesh is fine enough (in the sense that $h \ll \epsilon$) so that $\|\mathbf{u} - \mathbf{u}_h\|$ is sufficiently small and hence \mathbf{u}_h a sufficiently accurate reference solution. With the same argument, the accuracy of the coarse solution \mathbf{u}_H will not be satisfying as long as $H > \epsilon$. Note that reference problem (2) never needs to be solved. It just serves as a reference.

In the next section, we will construct the ideal multiscale space of the same (low) dimension as V_H , but which yields approximations that are of similar accuracy as the reference solution \mathbf{u}_h (in particular in the regime $H \gg \epsilon$). Throughout the paper, we do not consider errors that arise from numerical quadrature. For simplicity, we assume that all integrals can be computed exactly.

3 Ideal multiscale problem

In this section, we construct a low dimensional space that can capture the fine scale features of the true multiscale solution. We focus on constructing a good multiscale representation of the flux solution \mathbf{u} only. We call it ideal since the reference flux solution is in this space for all $f \in Q_H$. This should be contrasted to a localized multiscale space to be introduced in Section 4. In addition to the spaces V_h and V_H defined above we introduce the following detail space as the intersection of the fine space and the kernel of the coarse Raviart–Thomas interpolation operator,

$$V_h^f = \{\mathbf{v} \in V_h : \Pi_H \mathbf{v} = 0\}.$$

Since V_h^f is the kernel of a projection, it induces the splitting $V_h = V_H \oplus V_h^f$, where V_H is low dimensional and V_h^f is high dimensional. We refer to V_h^f as the detail space. In this section we aim at constructing a modified splitting, where V_H is replaced by a multiscale space which incorporates fine scale features.

3.1 Ideal multiscale space

We will construct the ideal multiscale space by applying fine scale correctors to all coarse functions in V_H , i.e. so that $(\text{Id} - G_h)(V_H)$ is the desired multiscale space for a linear

corrector operator G_h . The corrector operator is constructed using information from the coefficient \mathbf{A} , and has divergence free range in order to keep the flux conservation property of the coarse space.

The definition of the corrector requires us to construct the splitting $K_h = K_H \oplus K_h^f$ with

$$K_h^f := \{\mathbf{v} \in K_h : \Pi_H \mathbf{v} = 0\}, \quad \text{and} \quad K_H := \text{Range}((\Pi_H)|_{K_h}).$$

Next, we introduce an ideal corrector operator. We distinguish between local (element-wise) correctors and a global corrector.

Definition 6 (Ideal corrector operators). *Let $a^T(\mathbf{u}, \mathbf{v}) := (\mathbf{A}^{-1}\mathbf{u}, \mathbf{v})_T$ for $T \in \mathcal{T}_H$. For each such $T \in \mathcal{T}_H$, we define an ideal element corrector operator $G_h^T : V \rightarrow K_h^f$ by the equation*

$$a(G_h^T \mathbf{v}, \mathbf{v}^f) = a^T(\mathbf{v}, \mathbf{v}^f) \quad (5)$$

for all $\mathbf{v}^f \in K_h^f$. Furthermore, we define the ideal global corrector operator by summing the local contributions, i.e. $G_h := \sum_{T \in \mathcal{T}_H} G_h^T$.

The ideal corrector operators are well-defined since equation (5) is guaranteed a unique solution by the Lax–Milgram theorem due to the coercivity and boundedness of $a(\cdot, \cdot)$ on K_h^f . Using the ideal global corrector operator, we can define the discrete multiscale function space by

$$V_{H,h}^{\text{ms}} := (\text{Id} - G_h)(V_H),$$

where Id is the identity operator. This space has the same dimension as V_H . Furthermore, it allows for the splitting $V_h = V_{H,h}^{\text{ms}} \oplus V_h^f$. Note that the ideal multiscale space is the orthogonal complement of K_h^f with respect to $a(\cdot, \cdot)$, i.e.

$$a(\mathbf{v}_{H,h}^{\text{ms}}, \mathbf{v}^f) = 0 \quad (6)$$

for all $\mathbf{v}_{H,h}^{\text{ms}} \in V_{H,h}^{\text{ms}}$ and $\mathbf{v}^f \in K_h^f$.

3.2 Ideal multiscale problem formulation

In this section, we use the previously defined ideal multiscale space to define a (preliminary) multiscale approximation. The ideal multiscale problem reads as follows.

Definition 7 (Ideal multiscale problem). *Find $\mathbf{u}_{H,h}^{\text{ms}} \in V_{H,h}^{\text{ms}}$ and $p_H \in Q_H$, such that*

$$\begin{aligned} a(\mathbf{u}_{H,h}^{\text{ms}}, \mathbf{v}_h) + b(\mathbf{v}_h, p_H) &= 0, \\ b(\mathbf{u}_{H,h}^{\text{ms}}, q_H) &= -(f, q_H), \end{aligned} \quad (7)$$

for all $\mathbf{v}_h \in V_{H,h}^{\text{ms}}$ and $q_H \in Q_H$.

Lemma 8 (Unique solution of the ideal multiscale problem). *Under Assumptions (A1)–(A3) and (B1)–(B3), the ideal multiscale problem (7) has a unique solution. In particular, we have*

$$\gamma(1 + \alpha^{-1}\beta)^{-1} \leq \inf_{q \in Q_H} \sup_{\mathbf{v} \in V_{H,h}^{\text{ms}}} \frac{b(\mathbf{v}, q)}{\|q\|_Q \|\mathbf{v}\|_V},$$

i.e. inf-sup stability independent of h and H .

Proof. We let $K_{H,h}^{\text{ms}} = \{\mathbf{v} \in V_{H,h}^{\text{ms}} : \nabla \cdot \mathbf{v} = 0\}$. The coercivity of $a(\cdot, \cdot)$ on $K_{H,h}^{\text{ms}}$ follows immediately from its coercivity on K_h since $K_{H,h}^{\text{ms}} \subset K_h$. The operator $\text{Id} - G_h$ is stable in V with constant $1 + \alpha^{-1}\beta$, since $\nabla \cdot G_h \mathbf{v} = 0$ and

$$\begin{aligned} \|G_h \mathbf{v}\|_{L^2(\Omega)}^2 &\leq \alpha^{-1} a(G_h \mathbf{v}, G_h \mathbf{v}) \\ &= \alpha^{-1} a(\mathbf{v}, G_h \mathbf{v}) \\ &\leq \alpha^{-1} \beta \|\mathbf{v}\|_{L^2(\Omega)} \|G_h \mathbf{v}\|_{L^2(\Omega)} \end{aligned}$$

for all $\mathbf{v} \in V$. Combining these results with the inf-sup stability of $b(\cdot, \cdot)$ on V_H and Q_H , we get

$$\begin{aligned} \gamma &\leq \inf_{q \in Q_H} \sup_{\mathbf{v} \in V_H} \frac{b(\mathbf{v}, q)}{\|q\|_Q \|\mathbf{v}\|_V} \\ &\leq (1 + \alpha^{-1}\beta) \inf_{q \in Q_H} \sup_{\mathbf{v} \in V_H} \frac{(\nabla \cdot (\text{Id} - G_h) \mathbf{v}, q)}{\|q\|_Q \|(\text{Id} - G_h) \mathbf{v}\|_V} \\ &= (1 + \alpha^{-1}\beta) \inf_{q \in Q_H} \sup_{\mathbf{v} \in V_{H,h}^{\text{ms}}} \frac{(\nabla \cdot \mathbf{v}, q)}{\|q\|_Q \|\mathbf{v}\|_V}, \end{aligned} \tag{8}$$

i.e. $b(\cdot, \cdot)$ is inf-sup stable with constant $\gamma(1 + \alpha^{-1}\beta)^{-1}$ independent of H and h . We note that $K_{H,h}^{\text{ms}} = \{\mathbf{v} \in V_{H,h}^{\text{ms}} : b(\mathbf{v}, q_H) = 0 \ \forall q \in Q_H\}$, since $\nabla \cdot \mathbf{v} \in Q_H$ (see Remark 5). Finally, we apply Lemma 2 with $\mathcal{V} = V_{H,h}^{\text{ms}}$, $\mathcal{Q} = Q_H$, $\mathcal{K} = K_{H,h}^{\text{ms}}$ and constants $\tilde{\alpha} = \alpha$, $\tilde{\beta} = \beta$ and $\tilde{\gamma} = \gamma(1 + \alpha^{-1}\beta)^{-1}$. \square

3.3 Error estimate for ideal problem

In this section, we show that the flux solution of the ideal multiscale problem above converges in the energy norm with linear order in H to the reference solution. This convergence is independent of the variations of \mathbf{A} , i.e. we do not have any pre-asymptotic effects from the multiscale features.

Lemma 9 (Error estimate for ideal solution). *Under Assumptions (A1)–(A3) and (B1)–(B3), let \mathbf{u}_h solve (2) and $\mathbf{u}_{H,h}^{\text{ms}}$ solve (7), then*

$$\|\|\|\mathbf{u}_h - \mathbf{u}_{H,h}^{\text{ms}}\|\|\| \leq \beta^{1/2} C_{\hat{\Pi}} C_{\rho,d} H \|f - P_H f\|_{L^2(\Omega)}$$

where $C_{\rho,d}$ and $C_{\hat{\Pi}}$ are independent of h and H .

Proof. Parametrizing the solutions $\mathbf{u}_h(f)$ and $\mathbf{u}_{H,h}^{\text{ms}}(f)$ by the data f , we use the triangle inequality to obtain

$$\begin{aligned} \|\|\|\mathbf{u}_h(f) - \mathbf{u}_{H,h}^{\text{ms}}(f)\|\|\| \\ \leq \|\|\|\mathbf{u}_h(f) - \mathbf{u}_h(P_H f)\|\|\| + \|\|\|\mathbf{u}_h(P_H f) - \mathbf{u}_{H,h}^{\text{ms}}(P_H f)\|\|\| + \|\|\|\mathbf{u}_{H,h}^{\text{ms}}(P_H f) - \mathbf{u}_{H,h}^{\text{ms}}(f)\|\|\|. \end{aligned}$$

The two last terms will be shown to equal zero.

For the first term, we proceed in several steps. Let us define $\tilde{\mathbf{u}}_h := \mathbf{u}_h(f) - \mathbf{u}_h(P_H f) = \mathbf{u}_h(f - P_H f)$, which is the flux solution for the data $f - P_H f$. The corresponding pressure solution shall be denoted by \tilde{p}_h . First, we observe

$$\|\|\|\tilde{\mathbf{u}}_h\|\|\|^2 = (f - P_H f, \tilde{p}_h) = (f - P_H f, \tilde{p}_h - P_H \tilde{p}_h) \leq \|f - P_H f\|_{L^2(\Omega)} \|\tilde{p}_h - P_H \tilde{p}_h\|_{L^2(\Omega)}. \tag{9}$$

In order to bound the term $\|\tilde{p}_h - P_H\tilde{p}_h\|_{L^2(\Omega)}$, we let $\phi \in H_0^1(\Omega)$ be the weak solution to $\Delta\phi = \tilde{p}_h - P_H\tilde{p}_h$. Then we have

$$|\phi|_{H^1(\Omega)}^2 = (\tilde{p}_h - P_H\tilde{p}_h, \phi - P_H\phi) \leq C_{\rho,d}H\|\tilde{p}_h - P_H\tilde{p}_h\|_{L^2(\Omega)}|\phi|_{H^1(\Omega)}.$$

Defining $\mathbf{w} := \nabla\phi$ we get $\nabla \cdot \mathbf{w} = \tilde{p}_h - P_H\tilde{p}_h$ and $\|\mathbf{w}\|_{L^2(\Omega)} \leq C_{\rho,d}H\|\tilde{p}_h - P_H\tilde{p}_h\|_{L^2(\Omega)}$. Next, we use a pair of projection operators $\hat{\Pi}_h : V \rightarrow V_h$ and $\hat{P}_h : Q \rightarrow Q_h$ that commute with respect to the divergence operator, allows for \mathcal{T}_h to be non quasi-uniform, and where $\hat{\Pi}_h$ is L^2 -stable, i.e. $\hat{P}_h\nabla \cdot \mathbf{w} = \nabla \cdot \hat{\Pi}_h\mathbf{w}$ and $\|\hat{\Pi}_h\mathbf{w}\|_{L^2(\Omega)} \leq C_{\hat{\Pi}}\|\mathbf{w}\|_{L^2(\Omega)}$, with $C_{\hat{\Pi}}$ independent of h . The existence of such operators is proved in [11]. Exploiting this stability and the fact that $\tilde{p}_h - P_H\tilde{p}_h = \hat{P}_h(\nabla \cdot \mathbf{w})$ (since \hat{P}_h is a projection on Q_h and $\tilde{p}_h - P_H\tilde{p}_h \in Q_h$), we obtain

$$\begin{aligned} \|\tilde{p}_h - P_H\tilde{p}_h\|_{L^2(\Omega)}^2 &= (\tilde{p}_h - P_H\tilde{p}_h, \tilde{p}_h) = (\hat{P}_h(\nabla \cdot \mathbf{w}), \tilde{p}_h) \\ &= (\nabla \cdot \hat{\Pi}_h\mathbf{w}, \tilde{p}_h) = -(\mathbf{A}^{-1}\tilde{\mathbf{u}}_h, \hat{\Pi}_h\mathbf{w}) \leq \|\tilde{\mathbf{u}}_h\| \|\mathbf{A}^{-1/2}\hat{\Pi}_h\mathbf{w}\|_{L^2(\Omega)} \\ &\leq \beta^{1/2}C_{\hat{\Pi}}\|\tilde{\mathbf{u}}_h\| \|\mathbf{w}\|_{L^2(\Omega)} \leq \beta^{1/2}C_{\hat{\Pi}}C_{\rho,d}H\|\tilde{\mathbf{u}}_h\| \|\tilde{p}_h - P_H\tilde{p}_h\|_{L^2(\Omega)}. \end{aligned}$$

Combining this estimate with (9) yields

$$\|\tilde{\mathbf{u}}_h\|^2 \leq \beta^{1/2}C_{\hat{\Pi}}C_{\rho,d}H\|f - P_Hf\|_{L^2(\Omega)}\|\tilde{\mathbf{u}}_h\|.$$

For the second term, since the correctors are divergence free, we have $\nabla \cdot \mathbf{u}_{H,h}^{\text{ms}}(P_Hf) \in Q_H$. This implies $\nabla \cdot \mathbf{u}_{H,h}^{\text{ms}}(P_Hf) = -P_Hf$, hence

$$\nabla \cdot \mathbf{u}_{H,h}^{\text{ms}}(P_Hf) - \nabla \cdot \mathbf{u}_h(P_Hf) = 0,$$

i.e. $\mathbf{u}_{H,h}^{\text{ms}}(P_Hf) - \mathbf{u}_h(P_Hf) \in K_h$. Now, from first the equations in (2) and (7) in combination with the $a(\cdot, \cdot)$ -orthogonality between $V_{H,h}^{\text{ms}}$ and K_h^{f} , we get

$$\begin{aligned} a(\mathbf{u}_h(P_Hf), \mathbf{v}) &= 0, & \mathbf{v} \in V_h, & \quad \nabla \cdot \mathbf{v} = 0, \text{ and} \\ a(\mathbf{u}_{H,h}^{\text{ms}}(P_Hf), \mathbf{v}) &= 0, & \mathbf{v} \in V_{H,h}^{\text{ms}}, & \quad \nabla \cdot \mathbf{v} = 0, \text{ and} \\ a(\mathbf{u}_{H,h}^{\text{ms}}(P_Hf), \mathbf{v}) &= 0, & \mathbf{v} \in V_h^{\text{f}}, & \quad \nabla \cdot \mathbf{v} = 0. \end{aligned}$$

Since $V_h = V_{H,h}^{\text{ms}} \oplus V_h^{\text{f}}$, we obtain

$$a(\mathbf{u}_h(P_Hf) - \mathbf{u}_{H,h}^{\text{ms}}(P_Hf), \mathbf{v}) = 0,$$

for all $\mathbf{v} \in K_h$. Choosing $\mathbf{v} = \mathbf{u}_h(P_Hf) - \mathbf{u}_{H,h}^{\text{ms}}(P_Hf)$, we see that $\mathbf{u}_h(P_Hf) = \mathbf{u}_{H,h}^{\text{ms}}(P_Hf)$, thus the second term equals zero.

To show that the third term is zero, it is sufficient to show that $\mathbf{u}_{H,h}^{\text{ms}}(f - P_Hf) = 0$. The data $f - P_Hf$ is L^2 -orthogonal to the test space Q_H and it enters the equation (7) only in an L^2 scalar product with test functions. Hence $\mathbf{u}_{H,h}^{\text{ms}}(f - P_Hf) = \mathbf{u}_{H,h}^{\text{ms}}(P_H(f - P_Hf)) = 0$. \square

4 Localized multiscale method

The ideal corrector problems (5) are at least as expensive to solve as the original reference problem. Hence, we require to localize these problems to very small patches, without sacrificing the good approximation properties. If we can achieve this, the corrector problems

can be solved with low computational costs and fully in parallel. In this section, we show that this is indeed possible. We prove that we can truncate the computational domain Ω in the local corrector problems (5) to a small environment of a coarse element T . This is possible, since the solutions of (5) decay with exponential rate outside the coarse element T . We obtain a new localized corrector operator which can be used analogously to the ideal corrector operator to construct a localized multiscale space. This localization reduces the computational effort for assembling the multiscale space significantly.

In addition to the assumptions (A1)–(A3) and (B1)–(B3), we require additional assumptions on the computational domain and the mesh. More precisely we assume the following for the analysis.

(A4) We consider $d = 2$ and a simply-connected domain $\Omega \subset \mathbb{R}^2$.

(B4) The fine grid \mathcal{T}_h is quasi-uniform, i.e. the ratio between the maximum and the minimum diameter of a grid element is bounded by a generic constant.

We note that assumption (A4) is crucial for our proof. Assumption (B4) on the other hand could be dropped with a more careful analysis. In this case the estimates (and in particular the decay) will depend on the inverse of the minimum mesh size of the fine grid in a patch $U(T)$. For simplicity of the presentation, we do not elaborate this case and restrict ourselves to quasi-uniform meshes, i.e. to (B4). Note that even though we fix $d = 2$, we keep the general notation d to illustrate how the results are influenced by the dimension. The localized method can be formulated analogously for $d = 3$.

In order to localize the detail space K_h^f , we use admissible patches. We call this restriction to patches *localization*. For each $T \in \mathcal{T}_H$ we pick a connected patch $U(T)$ consisting of coarse grid elements and containing T . More precisely, for positive $k \in \mathbb{N}$ we define k -coarse-layer patches iteratively in the following way. For all $T \in \mathcal{T}_H$ (which are assumed to be closed sets), we define the element patch $U_k(T)$ in the coarse mesh \mathcal{T}_H by

$$\begin{aligned} U_0(T) &:= T, \\ U_k(T) &:= \bigcup \{T' \in \mathcal{T}_H : T' \cap U_{k-1}(T) \neq \emptyset\} \quad k = 1, 2, \dots \end{aligned} \tag{10}$$

See Figure 1 for an illustration of patches. For a given patch $U(T)$, we define the restriction of V_h^f to $U(T)$ by

$$V_h^f(U(T)) := \{\mathbf{w} \in V_h^f : \mathbf{w} = 0 \text{ in } \Omega \setminus U(T)\}.$$

Accordingly, we also define

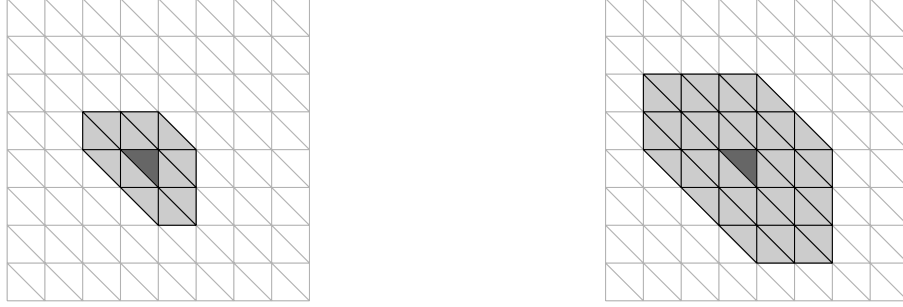
$$K_h^f(U(T)) := \{\mathbf{w} \in V_h^f(U(T)) : \nabla \cdot \mathbf{w} = 0\}.$$

Using this localized space, we define the localized corrector operators. Localized quantities are indexed by the patch layer size k .

Definition 10 (Localized corrector operators). *For each $T \in \mathcal{T}_H$ and $k \geq 1$ layers, we define a localized element corrector operator $G_{h,k}^T : V \rightarrow K_h^f(U_k(T))$:*

$$a(G_{h,k}^T \mathbf{v}, \mathbf{w}) = a^T(\mathbf{v}, \mathbf{w}) \tag{11}$$

for all $\mathbf{w} \in K_h^f(U_k(T))$. Further, we define the localized global corrector operator $G_{h,k} := \sum_{T \in \mathcal{T}_H} G_{h,k}^T$.



(a) One-coarse-layer patch, $k = 1$.

(b) Two-coarse-layer patch, $k = 2$.

Figure 1: Illustration of k -coarse-layer patches. Dark gray subdomain is T . Light gray subdomain is $U_k(T)$.

The localized corrector operators are again well-defined by the Lax-Milgram theorem, exploiting that $a(\cdot, \cdot)$ is a weighted L^2 -scalar product. Note that the definition of $K_h^f(U_k(T))$ implies Neumann boundary conditions on the localized corrector problems (11). We define a localized multiscale function space by

$$V_{H,h}^{\text{ms},k} := (\text{Id} - G_{h,k})(V_H)$$

and state the localized multiscale problem as follows.

Definition 11 (Localized multiscale problem). *The localized multiscale problem reads: find $\mathbf{u}_{H,h}^{\text{ms},k} \in V_{H,h}^{\text{ms},k}$ and $p_H \in Q_H$, such that*

$$\begin{aligned} a(\mathbf{u}_{H,h}^{\text{ms},k}, \mathbf{v}_h) + b(\mathbf{v}_h, p_H) &= 0, \\ b(\mathbf{u}_{H,h}^{\text{ms},k}, q_H) &= -(f, q_H), \end{aligned} \tag{12}$$

for all $\mathbf{v}_h \in V_{H,h}^{\text{ms},k}$ and $q_H \in Q_H$.

Definitions 10 and 11 constitute the proposed multiscale method. Next, we show that the above stated problem is well-posed.

Lemma 12 (Unique solution of localized multiscale problem). *Under Assumptions (A1)–(A3) and (B1)–(B3), the localized multiscale problem (12) has a unique solution for all k, h and H .*

Proof. We use similar arguments as in Lemma 8. The basic difference is that we need to show stability for the localized corrector operator $G_{h,k}$. We start with the stability of the localized element corrector operators. Here we have for arbitrary $\mathbf{v} \in V$

$$\| \| G_{h,k}^T \mathbf{v} \| \|^2 = a(G_{h,k}^T \mathbf{v}, G_{h,k}^T \mathbf{v}) = a^T(\mathbf{v}, G_{h,k}^T \mathbf{v}) \leq \| \mathbf{v} \|_T \| \| G_{h,k}^T \mathbf{v} \| \|. \tag{13}$$

Now, we can prove L^2 -stability of the localized global operator. We get

$$\begin{aligned}
\|G_{h,k}\mathbf{v}\|_{L^2(\Omega)}^2 &= \left\| \sum_{T \in \mathcal{T}_H} G_{h,k}^T \mathbf{v} \right\|_{L^2(\Omega)}^2 \leq \alpha^{-1} a \left(\sum_{T \in \mathcal{T}_H} G_{h,k}^T \mathbf{v}, \sum_{T' \in \mathcal{T}_H} G_{h,k}^{T'} \mathbf{v} \right) \\
&= \alpha^{-1} \sum_{T \in \mathcal{T}_H} \sum_{T' \subset U_k(T)} a(G_{h,k}^T \mathbf{v}, G_{h,k}^{T'} \mathbf{v}) \\
&\leq \frac{1}{2} \alpha^{-1} \sum_{T \in \mathcal{T}_H} \sum_{T' \subset U_k(T)} \left(\|G_{h,k}^T \mathbf{v}\|^2 + \|G_{h,k}^{T'} \mathbf{v}\|^2 \right) \\
&\leq \alpha^{-1} C_\rho k^d \sum_{T \in \mathcal{T}_H} \|G_{h,k}^T \mathbf{v}\|^2 \stackrel{(13)}{\leq} \alpha^{-1} C_\rho k^d \sum_{T \in \mathcal{T}_H} \|\mathbf{v}\|_T^2 \leq \alpha^{-1} \beta C_\rho k^d \|\mathbf{v}\|_{L^2(\Omega)}^2,
\end{aligned}$$

where C_ρ is a constant only depending on the shape regularity constant ρ of the coarse mesh. Similar to (8) we derive inf-sup stability with

$$\begin{aligned}
\gamma &\leq \inf_{q \in Q_H} \sup_{\mathbf{v} \in V_H} \frac{b(\mathbf{v}, q)}{\|q\|_Q \|\mathbf{v}\|_V} \\
&\leq (1 + \alpha^{-1/2} \beta^{1/2} C_\rho^{1/2} k^{d/2}) \inf_{q \in Q_H} \sup_{\mathbf{v} \in V_{H,h}^{\text{ms},k}} \frac{b(\mathbf{v}, q)}{\|q\|_Q \|\mathbf{v}\|_V}.
\end{aligned}$$

Observe that the inf-sup stability constant $\gamma_k^0 := \gamma(1 + \alpha^{-1/2} \beta^{1/2} C_\rho^{1/2} k^{d/2})^{-1}$ depends on k this time. \square

The inf-sup stability constant γ_k^0 depends on k due to overlapping patches. We come back to another estimate of the inf-sup stability constant in Section 4.3 after proving the decay of the correctors.

It is important to note that in the localized case we do not have orthogonality between $V_{H,h}^{\text{ms},k}$ and K_h^f as in the ideal case (cf. equation (6)). This orthogonality was crucial in the error estimate for the ideal method presented in Lemma 9. In the localized case, we rely on the exponential decay of the localized element correctors, which justifies localization to patches.

4.1 Error estimate for localized problem

In this section we state the main result of this paper, which is an a priori error estimate in the energy norm between the reference solution and the localized multiscale approximation. We first present a logarithmic stability result for the nodal Raviart–Thomas interpolation operator Π_H for fine scale functions and then state a lemma on the exponential decay of the correctors. Then the main theorem follows. The proof of the exponential decay is contained in Section 4.2. The notation $a \lesssim b$ stands for $a \leq Cb$ with some constant C that might depend on d , Ω , α , β and coarse and fine mesh regularity constants, but not on the mesh sizes h and H . In particular it does not depend on the possibly rapid oscillations in \mathbf{A} .

We recall a well known stability result for the nodal Raviart–Thomas interpolation operator.

Lemma 13 (Logarithmic stability of the nodal interpolation operator for divergence free functions). *Assume (B1)–(B4). For any given element $T \in \mathcal{T}_H$ there exists a constant C that only depends on the regularity of T and the quasi-uniformity of \mathcal{T}_h , such that*

$$\|\Pi_H \mathbf{v}_h\|_{L^2(T)}^2 \leq C \lambda(H/h)^2 \|\mathbf{v}_h\|_{L^2(T)}^2,$$

with $\lambda(H/h) := (1 + \log(H/h))^{1/2}$ for all $\mathbf{v}_h \in V_h$ with $\nabla \cdot \mathbf{v}_h = 0$.

A proof for this can be found in [34, Lemma 4.1]. This result holds for both $d = 2$ and 3.

Remark 14. *There exist unconditionally L^2 -stable Clément-type interpolation operators for which we could define $\lambda(H/h) := 1$ for all h and H instead, see [7, 10, 11, 32]. In particular, the operators introduced in [7, 11] are projections and were used as a technical tool in the proof of Lemma 9 above. However, these operators are hard to implement in practice and hence are not used in the proposed numerical method.*

Lemma 15 (Exponential decay of correctors). *Under Assumptions (A1)–(A4) and (B1)–(B4), there exists a generic constant $0 < \theta < 1$ depending on the contrast β/α , but not on h or H such that for all positive $k \in \mathbb{N}$:*

$$\left\| \sum_{T \in \mathcal{T}_H} (G_h^T \mathbf{v} - G_{h,k}^T \mathbf{v}) \right\|^2 \lesssim k^d \lambda(H/h)^2 \theta^{2k/\lambda(H/h)} \sum_{T \in \mathcal{T}_H} \|G_h^T \mathbf{v}\|^2 \quad (14)$$

for all $\mathbf{v} \in V$.

Proof. The lemma is a direct consequence of Lemma 21 in Section 4.2. \square

Now, combining the error estimate for the ideal multiscale method in Lemma 9 and Lemma 15 we get the following a priori error estimate of the localized multiscale method.

Theorem 16 (Error estimate for localized multiscale solution). *Under Assumptions (A1)–(A4) and (B1)–(B4), for a positive $k \in \mathbb{N}$, let \mathbf{u}_h solve (2) and $\mathbf{u}_{H,h}^{\text{ms},k}$ solve (12), then*

$$\left\| \mathbf{u}_h - \mathbf{u}_{H,h}^{\text{ms},k} \right\| \lesssim H \|f - P_H f\|_{L^2(\Omega)} + k^{d/2} \lambda(H/h)^2 \theta^{k/\lambda(H/h)} \|f\|_{L^2(\Omega)}, \quad (15)$$

for some $0 < \theta < 1$ depending on the contrast β/α , but not on k , h and H .

Before stating the proof, we discuss the role and choice of k . The second term in the error estimate (15) is an effect of the localization. This term can be made small by choosing large values of k , i.e. large patch sizes. A natural question is how to choose k to make the second term of order H to some power.

We write $\lambda = \lambda(H/h)$ for convenience. Let $\tilde{k} = 2d^{-1} \log(\theta) \lambda^{-1} k = -C_\theta \lambda^{-1} k$, where $C_\theta = -2d^{-1} \log(\theta) > 0$ is a constant independent of H and h . We are interested in the asymptotic behavior, so we consider $H \ll 1$. Setting the second term in (15) equal to $H \|f\|_{L^2(\Omega)}$ yields

$$\tilde{k} e^{\tilde{k}} = -C_\theta \lambda^{-4/d-1} H^{2/d},$$

that is $\tilde{k} = W(-C_\theta \lambda^{-4/d-1} H^{2/d})$, where W is the Lambert W -function. In terms of the number of layers k , we get $k = -C_\theta^{-1} \lambda W(-C_\theta \lambda^{-4/d-1} H^{2/d})$. This equation has two solutions for sufficiently small H . Since we require $k \geq 1$, we pick the branch $W \leq -1$.

Another, more practical option is to choose $k = R\lambda \log(1/H)$ for some constant R . Then the expression $k^{d/2}\lambda\theta^{k/\lambda}$ will be asymptotically (as $H \rightarrow 0$) dominated by the power $H^{-R\log\theta}$. Choosing R sufficiently large yields arbitrary order of accuracy of the term. The fine mesh size h is often fixed and we can choose

$$k = (1 + |\log_r(H)|)^{1/2} \log_s(1/H) \quad (16)$$

for some bases r and s of the two logarithms.

Remark 17. *If Clément-type interpolation operators are used, we have $\lambda \equiv 1$ independent of H/h . Choosing $k = C \log(1/H)$ makes the second term in (15) proportional to $\log(1/H)^{d/2} H^{-C \log\theta}$. For an appropriate C we can make the first term in (15) dominate the error estimate.*

Proof of Theorem 16. Let $\tilde{\mathbf{u}}_{H,h}^{\text{ms},k} := ((\text{Id} - G_{h,k}) \circ \Pi_H) \mathbf{u}_{H,h}^{\text{ms}} \in V_{H,h}^{\text{ms},k}$, then $\tilde{\mathbf{u}}_{H,h}^{\text{ms},k} - \mathbf{u}_{H,h}^{\text{ms},k}$ is divergence free. Hence, by Galerkin orthogonality we have

$$a(\mathbf{u}_h - \mathbf{u}_{H,h}^{\text{ms},k}, \mathbf{u}_h - \mathbf{u}_{H,h}^{\text{ms},k}) = a(\mathbf{u}_h - \mathbf{u}_{H,h}^{\text{ms},k}, \mathbf{u}_h - \tilde{\mathbf{u}}_{H,h}^{\text{ms},k})$$

and obtain

$$\left\| \mathbf{u}_h - \mathbf{u}_{H,h}^{\text{ms},k} \right\| \leq \left\| \mathbf{u}_h - \tilde{\mathbf{u}}_{H,h}^{\text{ms},k} \right\| \leq \left\| \mathbf{u}_h - \mathbf{u}_{H,h}^{\text{ms}} \right\| + \left\| \mathbf{u}_{H,h}^{\text{ms}} - \tilde{\mathbf{u}}_{H,h}^{\text{ms},k} \right\|.$$

The first term can be bounded by $\beta^{1/2} C_{\hat{\Pi}} C_{\rho,d} H \|f - P_H f\|_{L^2(\Omega)}$ by Lemma 9. Regarding the second term, using [34, Lemma 4.1] and stability of the ideal multiscale solution, we get

$$\sum_{T \in \mathcal{T}_H} \left\| G_h^T \Pi_H \mathbf{u}_{H,h}^{\text{ms}} \right\|^2 \leq \sum_{T \in \mathcal{T}_H} \left\| \Pi_H \mathbf{u}_{H,h}^{\text{ms}} \right\|_T^2 = \left\| \Pi_H \mathbf{u}_{H,h}^{\text{ms}} \right\|^2 \lesssim \lambda (H/h)^2 \|f\|_{L^2(\Omega)}^2$$

and can combine this with Lemma 15 to get

$$\begin{aligned} \left\| \mathbf{u}_{H,h}^{\text{ms}} - \tilde{\mathbf{u}}_{H,h}^{\text{ms},k} \right\| &= \left\| (G_{h,k} - G_h) \Pi_H \mathbf{u}_{H,h}^{\text{ms}} \right\| \\ &= \left\| \sum_{T \in \mathcal{T}_H} (G_{h,k}^T - G_h^T) \Pi_H \mathbf{u}_{H,h}^{\text{ms}} \right\| \\ &\lesssim k^{d/2} \lambda (H/h) \theta^{k/\lambda(H/h)} \left(\sum_{T \in \mathcal{T}_H} \left\| G_h^T \Pi_H \mathbf{u}_{H,h}^{\text{ms}} \right\|^2 \right)^{1/2} \\ &\lesssim k^{d/2} \lambda (H/h)^2 \theta^{k/\lambda(H/h)} \|f\|_{L^2(\Omega)}. \end{aligned}$$

□

4.2 Proof of exponential decay of correctors

This section consists of four lemmas, Lemma 18–21, of which the last one is the main result. The two first lemmas are auxiliary and are motivated by steps in the proofs of the latter two. Before starting, we need to set some notation and introduce some tools. We use the notation $W_{\text{loc}}^{1,2}(\mathbb{R}^d) = \{f : f \in H^1(\omega) \forall \text{ compact subsets } \omega \subset \mathbb{R}^d\}$. Note that we will use the letter K to denote arbitrary triangles of the coarse mesh \mathcal{T}_H . The first lemma says that every divergence free function \mathbf{w} in $H(\text{div}, \Omega)$ is the divergence of a skew-symmetric matrix.

Lemma 18. *Let Ω be a simply connected domain with Lipschitz boundary and let $\mathbf{w} \in H(\operatorname{div}, \Omega)$ with $\nabla \cdot \mathbf{w} = 0$ in Ω . Then there exists a skew-symmetric matrix $\psi \in [W_{\operatorname{loc}}^{1,2}(\mathbb{R}^d)]^{d \times d}$ with $\nabla \psi_{ij} \in [L^2(\mathbb{R}^d)]^d$ and $\int_{\Omega} \psi = 0$ such that*

$$\mathbf{w} = \nabla \cdot \psi \quad \text{in } \Omega \quad \text{and} \quad \|\nabla \psi_{ij}\|_{L^2(\omega)} \lesssim \|\mathbf{w}\|_{L^2(\omega)} \quad \text{for } \omega \subset \Omega. \quad (17)$$

Here, the divergence of ψ is defined along the rows.

Note that the above lemma is the only instance, where we require the restriction $d = 2$. Even though the existence of the skew-symmetric matrix is also available for $d = 3$, we could not prove localized estimates of the type $\|\nabla \psi_{ij}\|_{L^2(\omega)} \lesssim \|\mathbf{w}\|_{L^2(\omega)}$.

Proof. The result is a combination of well-known results. First, we extend the divergence-free vector field $\mathbf{w} \in H(\operatorname{div}, \Omega)$ to a divergence-free vector field $\tilde{\mathbf{w}} \in H(\operatorname{div}, \mathbb{R}^d)$. In particular we have $\tilde{\mathbf{w}} \in [L^2(\mathbb{R}^d)]^d$ and $\tilde{\mathbf{w}} = \mathbf{w}$ in Ω . Note that the extension of \mathbf{w} to \mathbb{R}^d will be typically not zero outside of Ω . The existence of such an extension operator was proved in [33, Proposition 3.8]. It is well known that there exists a skew-symmetric matrix $\psi \in [W_{\operatorname{loc}}^{1,2}(\mathbb{R}^d)]^{d \times d}$ with $\nabla \psi_{ij} \in [L^2(\mathbb{R}^d)]^d$, such that $\tilde{\mathbf{w}} = \nabla \cdot \psi$ (see [23, Lemma 2.3]). The matrix is only unique up to a constant, so we fix the constant by $\int_{\Omega} \psi = 0$ (which gives us a Poincaré inequality). The inequality $\|\nabla \psi_{ij}\|_{L^2(\omega)} \lesssim \|\tilde{\mathbf{w}}\|_{L^2(\omega)}$ (for $\omega \subset \mathbb{R}^d$) can be seen as follows for $d = 2$. Obviously, if $i = j$ we obtain $\nabla \psi_{ii} = \nabla \psi_{jj} = 0$ and estimate (17) is trivial. If $i \neq j$, we obtain by using the skew-symmetry

$$\begin{aligned} \|\mathbf{w}\|_{L^2(\omega)}^2 &= \|\nabla \cdot \psi\|_{L^2(\omega)}^2 = \|\partial_1 \psi_{11} + \partial_2 \psi_{12}\|_{L^2(\omega)}^2 + \|\partial_1 \psi_{21} + \partial_2 \psi_{22}\|_{L^2(\omega)}^2 \\ &= \|\partial_2 \psi_{12}\|_{L^2(\omega)}^2 + \|\partial_1 \psi_{21}\|_{L^2(\omega)}^2 = \|\partial_2 \psi_{12}\|_{L^2(\omega)}^2 + \|\partial_1 \psi_{12}\|_{L^2(\omega)}^2 \\ &= \|\nabla \psi_{12}\|_{L^2(\omega)}^2 = \|\nabla \psi_{21}\|_{L^2(\omega)}^2, \end{aligned}$$

i.e. we obtain even equality in estimate (17). \square

We also require suitable cut-off functions that are central for the proof. For $T \in \mathcal{T}_H$ and positive $k \in \mathbb{N}$, we let the function $\eta_{T,k} \in P_1(\mathcal{T}_H)$ (globally continuous and piecewise linear w.r.t. \mathcal{T}_H) be defined as

$$\begin{aligned} \eta_{T,k}(x) &= 0 \quad \text{for } x \in U_{k-1}(T), \\ \eta_{T,k}(x) &= 1 \quad \text{for } x \in \Omega \setminus U_k(T). \end{aligned} \quad (18)$$

We start with the following lemma, which enables us to approximate truncated functions from K_h^f .

Lemma 19. *Let $\mathbf{w}_h \in K_h^f$ and let $\psi \in [W_{\operatorname{loc}}^{1,2}(\Omega)]^{d \times d}$ with $\mathbf{w}_h = \nabla \cdot \psi$ denote the corresponding skew-symmetric matrix as in Lemma 18. Let furthermore $\psi_K := |K|^{-1} \int_K \psi$ denote the average on $K \in \mathcal{T}_H$ and let $\psi_H \in [L^2(\Omega)]^{d \times d}$ denote the corresponding piecewise constant matrix with $\psi_H(x) = \psi_K$ for $x \in K$. The broken divergence-operator $\nabla_H \cdot$ is given by $\nabla_H \cdot v := \nabla \cdot v|_K$ for $K \in \mathcal{T}_H$. The function $\eta_{T,k} \in P_1(\mathcal{T}_H)$ is a given cut-off function as defined in (18) for $k > 0$. Then, we have that the function $\tilde{\mathbf{w}}_h := \Pi_h(\nabla \cdot (\eta_{T,k} \psi)) - (\Pi_H \circ \Pi_h)(\nabla \cdot (\eta_{T,k} \psi)) \in K_h^f$ fulfills the following estimate for any $K \in \mathcal{T}_H$:*

$$\begin{aligned} \|\nabla \cdot (\eta_{T,k} \psi) - \nabla_H \cdot (\eta_{T,k} \psi_H) - \tilde{\mathbf{w}}_h\|_{L^2(K)} &\lesssim \begin{cases} \lambda(H/h) \|\mathbf{w}_h\|_{L^2(K)} & K \subset U_k(T) \setminus U_{k-1}(T) \\ 0 & \text{otherwise.} \end{cases} \end{aligned}$$

Obviously we also have $\text{supp}(\tilde{\mathbf{w}}_h) \subset \Omega \setminus U_{k-1}(T)$.

Proof. First, we observe that the skew-symmetric matrix ψ must be a polynomial of maximum degree 2 on each fine grid element. We use this in the following without mentioning.

We fix the element $T \in \mathcal{T}_H$ and $k \in \mathbb{N}$ and denote $\eta := \eta_{T,k}$. Furthermore, we define for $K \in \mathcal{T}_H$

$$c_K := |K|^{-1} \int_K \eta \quad \text{and} \quad \psi_K := |K|^{-1} \int_K \psi.$$

We define $\tilde{\mathbf{w}}_h := \Pi_h(\nabla \cdot (\eta\psi)) - (\Pi_H \circ \Pi_h)(\nabla \cdot (\eta\psi))$ and observe that $\tilde{\mathbf{w}}_h \in K_h^f$ and $\mathbf{w}_h = \tilde{\mathbf{w}}_h$ on $\Omega \setminus U_k(T)$. The property $\Pi_H(\tilde{\mathbf{w}}_h) = 0$ is clear. The property $\nabla \cdot \tilde{\mathbf{w}}_h = 0$ follows from the fact that $\eta\psi$ is still skew symmetric and that $\nabla \cdot (\Pi_H \circ \Pi_h)(\cdot) = (P_H \circ P_h)(\nabla \cdot \cdot)$. Since ψ_K and c_K are constant on K we have

$$\Pi_h(\nabla \cdot (c_K\psi_K)) = \nabla \cdot (c_K\psi_K) = 0 \quad \text{on } K. \quad (19)$$

Furthermore, since $\Pi_H(\mathbf{v}_H) = \mathbf{v}_H$ for all $\mathbf{v}_H \in V_H$ and since $\nabla \cdot (\eta\psi_K) \in V_H$ we also have

$$(\Pi_H \circ \Pi_h)(\nabla \cdot (\eta\psi_K)) = \Pi_h(\nabla \cdot (\eta\psi_K)) \quad \text{on } K. \quad (20)$$

Finally, we also have on K ,

$$(\Pi_H \circ \Pi_h)(\nabla \cdot (c_K\psi)) = c_K(\Pi_H \circ \Pi_h)(\nabla \cdot \psi) = c_K\Pi_H(\mathbf{w}_h) = 0. \quad (21)$$

Combining (19), (20), and (21) we obtain for every $K \in \mathcal{T}_H$

$$\begin{aligned} & \|(\Pi_H \circ \Pi_h)(\nabla \cdot (\eta\psi)) - \Pi_h(\nabla \cdot (\eta\psi_K))\|_{L^2(K)} \\ &= \|(\Pi_H \circ \Pi_h)(\nabla \cdot (\eta\psi) - \nabla \cdot (c_K\psi) - \nabla \cdot (\eta\psi_K) + \nabla \cdot (c_K\psi_K))\|_{L^2(K)} \\ &= \|(\Pi_H \circ \Pi_h)(\nabla \cdot ((\eta - c_K)(\psi - \psi_K)))\|_{L^2(K)}. \end{aligned} \quad (22)$$

Now, we consider the quantity we want to estimate. For any $K \in \mathcal{T}_H$,

$$\begin{aligned} & \|\nabla \cdot (\eta\psi) - \nabla_H \cdot (\eta\psi_H) - \tilde{\mathbf{w}}_h\|_{L^2(K)} \\ & \leq \|\nabla \cdot (\eta(\psi - \psi_K)) - \Pi_h(\nabla \cdot (\eta(\psi - \psi_K)))\|_{L^2(K)} \\ & \quad + \|\Pi_h(\nabla \cdot (\eta(\psi - \psi_K))) - \Pi_h(\nabla \cdot (\eta\psi)) + (\Pi_H \circ \Pi_h)(\nabla \cdot (\eta\psi))\|_{L^2(K)} \\ & = \|\nabla \cdot (\eta(\psi - \psi_K)) - \Pi_h(\nabla \cdot (\eta(\psi - \psi_K)))\|_{L^2(K)} \\ & \quad + \|(\Pi_H \circ \Pi_h)(\nabla \cdot (\eta\psi)) - \Pi_h(\nabla \cdot (\eta\psi_K))\|_{L^2(K)} \\ & \stackrel{(22)}{=} \|\nabla \cdot ((\eta - c_K)(\psi - \psi_K)) - \Pi_h(\nabla \cdot ((\eta - c_K)(\psi - \psi_K)))\|_{L^2(K)} \\ & \quad + \|(\Pi_H \circ \Pi_h)(\nabla \cdot ((\eta - c_K)(\psi - \psi_K)))\|_{L^2(K)} \\ & \lesssim \lambda(H/h)\|\nabla \cdot ((\eta - c_K)(\psi - \psi_K))\|_{L^2(K)}. \end{aligned} \quad (23)$$

In the last step we used Lemma 13, the property that $\Pi_h \nabla \cdot ((\eta - c_K)(\psi - \psi_K))$ is divergence free and the fact that Π_h is locally L^2 -stable when applied to functions of

small fixed polynomial degree, i.e. for fixed $t \in \mathcal{T}_h$ and $r \in \mathbb{N}$ there exists a constant $C(r)$ that only depends on r and the shape regularity of t such that

$$\|\Pi_h(\mathbf{v})\|_{L^2(t)} \leq C(r)\|\mathbf{v}\|_{L^2(t)} \quad \text{for all } \mathbf{v} \in [\mathbb{P}^r(t)]^d.$$

Continuing from (23) we obtain

$$\begin{aligned} & \|\nabla \cdot ((\eta - c_K)(\psi - \psi_K))\|_{L^2(K)}^2 \\ & \lesssim \|(\eta - c_K)\nabla \cdot \psi\|_{L^2(K)}^2 + \|(\psi - \psi_K)\nabla\eta\|_{L^2(K)}^2 \\ & \lesssim H^2\|\nabla\eta\|_{L^\infty(K)}^2\|\nabla\psi\|_{L^2(K)}^2 \\ & \stackrel{(17)}{\lesssim} \begin{cases} \|\mathbf{w}\|_{L^2(K)}^2 & K \subset U_k(T) \setminus U_{k-1}(T) \\ 0 & \text{otherwise.} \end{cases} \end{aligned} \quad (24)$$

Note that we used the properties of η to obtain the Lipschitz bound $\|\eta - c_K\|_{L^\infty(K)} \lesssim H\|\nabla\eta\|_{L^\infty(K)} \lesssim 1$ and that $\nabla\eta$ has no support outside $U_k(T) \setminus U_{k-1}(T)$. We also used the Poincaré inequality for $\eta - c_K$ which has a zero average on K . Combining (23) and (24) yields the sought result. \square

We continue with a lemma showing the exponential decay of solutions to problems of the form in (5).

Lemma 20. *Now, let $\mathbf{w}^T \in K_h^f$ be the solution of*

$$\int_{\Omega} \mathbf{A}^{-1}\mathbf{w}^T \cdot \mathbf{v}_h = F_T(\mathbf{v}_h) \quad \text{for all } \mathbf{v}_h \in K_h^f \quad (25)$$

where $F_T \in (K_h^f)'$ is such that $F_T(\mathbf{v}_h) = 0$ for all $\mathbf{v}_h \in K_h^f(\Omega \setminus T)$. Then, there exists a generic constant $0 < \theta < 1$ (depending on the contrast β/α) such that for all positive $k \in \mathbb{N}$:

$$\|\|\mathbf{w}^T\|\|_{\Omega \setminus U_k(T)} \lesssim \theta^{k/\lambda(H/h)} \|\|\mathbf{w}^T\|\|_{\Omega}. \quad (26)$$

Proof. The proof exploits similar arguments as in [30]. Let us fix $k \in \mathbb{N}$. We denote again $\eta := \eta_{T,k} \in P_1(\mathcal{T}_H)$ (as in (18)). We apply Lemma 19 to $\mathbf{w}^T \in K_h^f$. The corresponding skew symmetric matrix shall again be denoted by $\psi = \psi(\mathbf{w}^T)$ and we define

$$\tilde{\mathbf{w}}^T := \Pi_h(\nabla \cdot (\eta\psi)) - (\Pi_H \circ \Pi_h)(\nabla \cdot (\eta\psi)).$$

We obtain that $\nabla \cdot (\eta\psi) - \nabla_H \cdot (\eta\psi_H) - \tilde{\mathbf{w}}^T$ is zero outside $U_k(T) \setminus U_{k-1}(T)$ and

$$\|\nabla \cdot (\eta\psi) - \nabla_H \cdot (\eta\psi_H) - \tilde{\mathbf{w}}^T\|_{L^2(U_k(T) \setminus U_{k-1}(T))} \lesssim \lambda(H/h)\|\mathbf{w}^T\|_{L^2(U_k(T) \setminus U_{k-1}(T))}. \quad (27)$$

First observe that

$$\int_{\Omega \setminus U_{k-1}(T)} \mathbf{A}^{-1}\mathbf{w}^T \cdot \tilde{\mathbf{w}}^T = \int_{\Omega} \mathbf{A}^{-1}\mathbf{w}^T \cdot \tilde{\mathbf{w}}^T = F_T(\tilde{\mathbf{w}}^T) = 0 \quad (28)$$

and

$$\eta\mathbf{w}^T = \eta\nabla \cdot \psi = \nabla \cdot (\eta\psi) - \psi\nabla\eta. \quad (29)$$

With that we have

$$\begin{aligned}
\int_{\Omega \setminus U_k(T)} \mathbf{A}^{-1} \mathbf{w}^T \cdot \mathbf{w}^T &\leq \int_{\Omega \setminus U_{k-1}(T)} \mathbf{A}^{-1} \mathbf{w}^T \cdot (\eta \mathbf{w}^T) \\
&\stackrel{(29)}{=} \int_{\Omega \setminus U_{k-1}(T)} \mathbf{A}^{-1} \mathbf{w}^T \cdot (\nabla \cdot (\eta \psi) - \psi \nabla \eta) \\
&\stackrel{(28)}{=} \int_{\Omega \setminus U_{k-1}(T)} \mathbf{A}^{-1} \mathbf{w}^T \cdot (\nabla \cdot (\eta \psi) - \psi \nabla \eta - \tilde{\mathbf{w}}^T) \\
&= \underbrace{\int_{\Omega \setminus U_{k-1}(T)} \mathbf{A}^{-1} \mathbf{w}^T \cdot (\nabla \cdot (\eta \psi) - \nabla_H \cdot (\eta \psi_H) - \tilde{\mathbf{w}}^T)}_{=: \text{I}} \\
&\quad + \underbrace{\int_{\Omega \setminus U_{k-1}(T)} \mathbf{A}^{-1} \mathbf{w}^T \cdot (\nabla_H \cdot (\eta \psi_H) - \psi \nabla \eta)}_{=: \text{II}}.
\end{aligned}$$

For I we use (27) to obtain

$$\text{I} \lesssim \lambda(H/h) \left\| \left\| \mathbf{w}^T \right\| \right\|_{U_k(T) \setminus U_{k-1}(T)}^2$$

and for II we obtain

$$\begin{aligned}
\text{II} &= \int_{\Omega \setminus U_{k-1}(T)} \mathbf{A}^{-1} \mathbf{w}^T \cdot ((\psi_H - \psi) \nabla \eta) \\
&\lesssim \sum_{\substack{K \in \mathcal{T}_H \\ K \subset U_k(T) \setminus U_{k-1}(T)}} \left\| \left\| \mathbf{w}^T \right\| \right\|_K H \|\nabla \eta\|_{L^\infty(K)} \|\nabla \psi\|_{L^2(K)} \\
&\lesssim \left\| \left\| \mathbf{w}^T \right\| \right\|_{U_k(T) \setminus U_{k-1}(T)}^2.
\end{aligned}$$

Now, denote by $L := C\lambda(H/h)$, and we get

$$\left\| \left\| \mathbf{w}^T \right\| \right\|_{\Omega \setminus U_k(T)}^2 \leq L \left\| \left\| \mathbf{w}^T \right\| \right\|_{U_k(T) \setminus U_{k-1}(T)}^2 \leq L \left(\left\| \left\| \mathbf{w}^T \right\| \right\|_{\Omega \setminus U_{k-1}(T)}^2 - \left\| \left\| \mathbf{w}^T \right\| \right\|_{\Omega \setminus U_k(T)}^2 \right)$$

where C is independent of T , k and \mathbf{A} , but can depend on the contrast. We obtain

$$\left\| \left\| \mathbf{w}^T \right\| \right\|_{\Omega \setminus U_k(T)}^2 \leq (1 + L^{-1})^{-1} \left\| \left\| \mathbf{w}^T \right\| \right\|_{\Omega \setminus U_{k-1}(T)}^2.$$

A recursive application of this inequality and $\left\| \left\| \mathbf{w}^T \right\| \right\|_{\Omega \setminus U_0(T)} \leq \left\| \left\| \mathbf{w}^T \right\| \right\|_{\Omega}$ yields

$$\left\| \left\| \mathbf{w}^T \right\| \right\|_{\Omega \setminus U_k(T)}^2 \leq e^{-\log(1+L^{-1})k} \left\| \left\| \mathbf{w}^T \right\| \right\|_{\Omega}^2 \leq e^{-\log(1+C^{-1})k/\lambda(H/h)} \left\| \left\| \mathbf{w}^T \right\| \right\|_{\Omega}^2,$$

where we used Bernoulli's inequality and that $0 < L^{-1} \leq C^{-1}$ in the last step. The choice $\theta := (1 + C^{-1})^{-1}$ proves the lemma. \square

The following lemma is the main result of this subsection. It can be directly applied to the localized corrector problems (11) with $F_T(\mathbf{v}_h) = a^T(\mathbf{v}, \mathbf{v}_h)$, $G_{h,k}^T \mathbf{v} = \mathbf{w}^{T,k}$ and $G_h^T \mathbf{v} = \mathbf{w}^T$ for any $\mathbf{v} \in V$.

Lemma 21. *Let the setting of Lemma 20 hold true and let additionally $\mathbf{w}^{T,k} \in K_h^f(U_k(T))$ denote the solution of*

$$\int_{U_k(T)} \mathbf{A}^{-1} \mathbf{w}^{T,k} \cdot \mathbf{v}_h = F_T(\mathbf{v}_h) \quad \text{for all } \mathbf{v}_h \in K_h^f(U_k(T)). \quad (30)$$

Then, there exists a generic constant $0 < \theta < 1$ (depending on the contrast) such that for all positive $k \in \mathbb{N}$:

$$\left\| \sum_{T \in \mathcal{T}_H} (\mathbf{w}^T - \mathbf{w}^{T,k}) \right\|_{\Omega}^2 \lesssim k^d \lambda(H/h)^2 \theta^{2k/\lambda(H/h)} \sum_{T \in \mathcal{T}_H} \|\mathbf{w}^T\|_{\Omega}^2. \quad (31)$$

Proof. Let $\eta_{T,k}$ be defined according to (18) and denote $\mathbf{z} := \sum_{T \in \mathcal{T}_H} (\mathbf{w}^T - \mathbf{w}^{T,k}) \in K_h^f$. We obtain

$$\|\mathbf{z}\|_{\Omega}^2 = \sum_{T \in \mathcal{T}_H} \underbrace{(\mathbf{A}^{-1}(\mathbf{w}^T - \mathbf{w}^{T,k}), (1 - \eta_{T,k+1})\mathbf{z})}_{=: \text{I}} + \underbrace{(\mathbf{A}^{-1}(\mathbf{w}^T - \mathbf{w}^{T,k}), \eta_{T,k+1}\mathbf{z})}_{=: \text{II}}.$$

The first term is estimated by

$$\text{I} \leq \|\mathbf{w}^T - \mathbf{w}^{T,k}\|_{\Omega} \|\mathbf{z}(1 - \eta_{T,k+1})\|_{U_{k+1}(T)} \leq \|\mathbf{w}^T - \mathbf{w}^{T,k}\|_{\Omega} \|\mathbf{z}\|_{U_{k+1}(T)}.$$

For the second term we have $\mathbf{z} \in K_h^f$, hence there exists again a skew-symmetric matrix $\psi = \psi(\mathbf{z})$ with the properties as in Lemma 18 with

$$\eta_{T,k+1}\mathbf{z} = \eta_{T,k+1}\nabla \cdot \psi = \nabla \cdot (\eta_{T,k+1}\psi) - \psi \nabla \eta_{T,k+1}.$$

We define $\tilde{\mathbf{z}} := \Pi_h(\nabla \cdot (\eta_{T,k+1}\psi)) - (\Pi_H \circ \Pi_h)(\nabla \cdot (\eta_{T,k+1}\psi))$. Using Lemma 19 and $\text{supp}(\eta_{T,k+1}\mathbf{z}) \cap \text{supp}(\mathbf{w}^{T,k}) = \emptyset$ we get

$$\begin{aligned} (\mathbf{A}^{-1}(\mathbf{w}^T - \mathbf{w}^{T,k}), \eta_{T,k+1}\mathbf{z}) &= (\mathbf{A}^{-1}\mathbf{w}^T, \eta_{T,k+1}\mathbf{z}) \\ &\stackrel{(28)}{=} \int_{\Omega \setminus U_k(T)} \mathbf{A}^{-1}\mathbf{w}^T \cdot (\nabla \cdot (\eta_{T,k+1}\psi) - \psi \nabla \eta_{T,k+1} - \tilde{\mathbf{z}}) \\ &= \int_{\Omega \setminus U_k(T)} \mathbf{A}^{-1}(\mathbf{w}^T - \mathbf{w}^{T,k}) \cdot (\nabla \cdot (\eta_{T,k+1}\psi) - \psi \nabla \eta_{T,k+1} - \tilde{\mathbf{z}}). \end{aligned}$$

Now proceed as in Lemma 20 to obtain

$$\text{II} \lesssim \lambda(H/h) \|\mathbf{w}^T - \mathbf{w}^{T,k}\|_{\Omega} \|\mathbf{z}\|_{U_{k+1}(T)}.$$

Combining the estimates for I and II and applying Hölder's inequality finally yields, for $k \geq 1$,

$$\begin{aligned} \|\mathbf{z}\|_{\Omega}^2 &\lesssim \lambda(H/h) \sum_{T \in \mathcal{T}_H} \|\mathbf{w}^T - \mathbf{w}^{T,k}\|_{\Omega} \|\mathbf{z}\|_{U_{k+1}(T)} \\ &\lesssim k^{\frac{d}{2}} \lambda(H/h) \left(\sum_{T \in \mathcal{T}_H} \|\mathbf{w}^T - \mathbf{w}^{T,k}\|_{\Omega}^2 \right)^{\frac{1}{2}} \|\mathbf{z}\|_{\Omega}. \end{aligned} \quad (32)$$

It remains to bound $\|\mathbf{w}^T - \mathbf{w}^{T,k}\|_{\Omega}^2$. In order to do this, we use Galerkin orthogonality for the local problems, which gives us

$$\|\mathbf{w}^T - \mathbf{w}^{T,k}\|_{\Omega}^2 \leq \inf_{\tilde{\mathbf{w}}^{T,k} \in K_h^i(U_k(T))} \|\mathbf{w}^T - \tilde{\mathbf{w}}^{T,k}\|_{\Omega}^2.$$

Again, we use Lemma 20 to show

$$\|\mathbf{w}^T - \mathbf{w}^{T,k}\|_{\Omega}^2 \lesssim \theta^{2k/\lambda(H/h)} \|\mathbf{w}^T\|_{\Omega}^2. \quad (33)$$

Combining (32) and (33) proves the lemma. \square

4.3 Inf-sup stability revisited

The decay results can be used to prove another inf-sup stability constant γ_k^1 in addition to γ_k^0 from Lemma 12 for the bilinear form $b(\cdot, \cdot)$ with the localized multiscale space. Using Lemma 21, we obtain

$$\begin{aligned} \|G_{h,k}\mathbf{v} - G_h\mathbf{v}\|_{L^2(\Omega)}^2 &= \left\| \sum_{T \in \mathcal{T}_H} (G_{h,k}^T \mathbf{v} - G_h^T \mathbf{v}) \right\|_{L^2(\Omega)}^2 \\ &\lesssim k^d \lambda(H/h)^2 \theta^{2k/\lambda(H/h)} \sum_{T \in \mathcal{T}_H} \|G_h^T \mathbf{v}\|_{L^2(\Omega)}^2 \\ &\lesssim k^d \lambda(H/h)^2 \theta^{2k/\lambda(H/h)} \|\mathbf{v}\|_{L^2(\Omega)}^2. \end{aligned}$$

We get the following stability

$$\begin{aligned} \|G_{h,k}\mathbf{v}\|_{L^2(\Omega)} &\leq \|G_{h,k}\mathbf{v} - G_h\mathbf{v}\|_{L^2(\Omega)} + \|G_h\mathbf{v}\|_{L^2(\Omega)} \\ &\lesssim (k^{d/2} \lambda(H/h) \theta^{k/\lambda(H/h)} + 1) \|\mathbf{v}\|_{L^2(\Omega)}. \end{aligned}$$

Using the same technique as in Lemma 12, we obtain an inf-sup stability constant $\gamma_k^1 := \gamma(2 + k^{d/2} \lambda(H/h) \theta^{k/\lambda(H/h)})^{-1}$.

For the nodal Raviart–Thomas interpolation operator Π_H , $\lambda(H/h)$ depends on h and H , and we cannot obtain a uniform bound on the constant for this estimate either. However, for L^2 -stable Clément-type interpolation operators (discussed in Remark 14), we have $\lambda(H/h) \equiv 1$, independently of h and H . If using such an interpolator in place of Π_H , the inf-sup stability constant γ_k^1 can be bounded from below by a positive constant independent of h and H , since $k^{d/2} \theta^k$ is bounded from above with respect to k .

5 Numerical experiments

Four numerical experiments are presented in this section. Their purpose is to show that the error estimate for the localized multiscale method presented in Theorem 16 is valid and useful for determining the patch sizes and that the method is competitive.

A brief overview of the implementation of the method follows. The two dimensional Raviart–Thomas finite element is used. For all free degrees of freedom e (interior edges), the localized global corrector $G_{h,k}\Phi_e$ for the corresponding basis function Φ_e is computed

according to equation (11). The additional constraints on the test and trial functions to be in the kernel to the coarse Raviart–Thomas projection operator are implemented using Lagrange multipliers (in addition to those already there due to the mixed formulation). The corrector problems are cheap since they are solved only on small patches. This can be done in parallel over all basis functions. Finally, problem (12) is solved. Regarding the linear system arising here, we compare it with the linear system arising from a standard Raviart–Thomas discretization (using V_H for the flux) of the mixed formulation on the coarse mesh:

$$\begin{pmatrix} \mathbf{K} & \mathbf{B}^T \\ \mathbf{B} & \mathbf{0} \end{pmatrix} = \begin{pmatrix} \mathbf{0} \\ \mathbf{b} \end{pmatrix},$$

for matrices \mathbf{K} and \mathbf{B} and a vector \mathbf{b} . The difference with the multiscale method is that matrix corresponding to the bilinear form $a(\cdot, \cdot)$ is computed using the low dimensional modified localized multiscale basis $\{\Phi_E - G_{h,k}\Phi_E\}_E$ spanning $V_{H,h}^{\text{ms},k}$. Since the correctors are divergence free, \mathbf{K} is replaced by a different matrix $\tilde{\mathbf{K}}$ in the system above, whereas \mathbf{B} and \mathbf{b} are left intact.

In all numerical experiments below, the diffusion matrix is diagonal with identical diagonal elements, $\mathbf{A}(x) = A(x)\mathbf{I}$, with \mathbf{I} being the identity matrix, for a scalar-valued function A .

5.1 Investigation of error from localization

In this experiment, we investigate how the error in energy norm of the localized multiscale solution is affected by the localization to patches of the correctors. The error due to localization is bounded by the second term in the estimate in Theorem 16. This term will be the focus of this experiment.

The computational domain is the unit square $\Omega = [0, 1]^2$ and the source function is given by

$$f(x) = \begin{cases} 1 & \text{if } x \in [0, 1/4]^2, \\ -1 & \text{if } x \in [3/4, 1]^2, \\ 0 & \text{otherwise.} \end{cases}$$

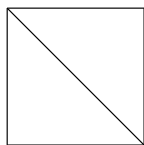
We consider three different diffusion coefficients A :

1. Constant: $A(x) = 1$ in the whole domain.
2. Noise: $A(x)$ is piecewise constant on a $2^7 \times 2^7$ uniform rectangular grid. In each grid cell, the value of A is equal to a realization of $\exp(10\omega)$, where ω is a cell-specific standard uniformly distributed variable.
3. Channels: $A(x)$ is as is shown in Figure 2. It is piecewise constant on a $2^7 \times 2^7$ uniform rectangular grid. The coefficient $A(x) = 1$ for x in black cells and $A(x) = \exp(10)$ for x in white cells.

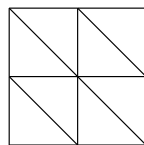
Figure 3 shows the mesh used in the experiment. Both fine and coarse meshes are constructed as shown in the figure. A reference solution \mathbf{u}_h was computed with the standard Raviart–Thomas spaces V_h and Q_h with $h = 2^{-8}$. Solutions $\mathbf{u}_{H,h}^{\text{ms},k}$ to the localized multiscale problem were computed using $H = 2^{-2}, 2^{-3}, \dots, 2^{-6}$. The patch size k was chosen



Figure 2: Coefficient A defined on a $2^7 \times 2^7$ grid of Ω .



(a) Coarsest mesh, $h = 1$.



(b) One refinement, $h = 1/2$.

Figure 3: Family of triangulations of the unit square.

as

$$k = C(1 + \log_2(H/h))^{1/2} \log_2(H^{-1})$$

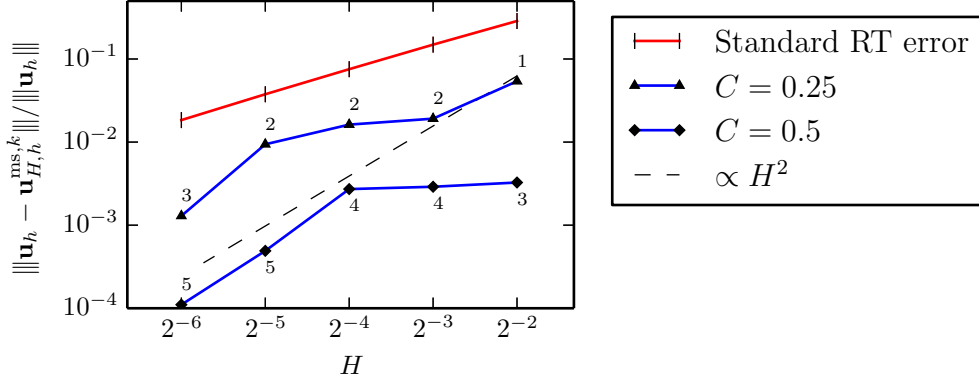
rounded to the nearest integer with $C = 0.25$ and $C = 0.5$. The relative error (using the reference solution in place of the exact solution) in energy norm, i.e. $\left\| \left\| \mathbf{u}_h - \mathbf{u}_{H,h}^{\text{ms},k} \right\| \right\| / \left\| \left\| \mathbf{u}_h \right\| \right\|$ was computed. See Figure 4 for the resulting convergence of this error with respect to H for the two values of C . Note that since $f \in Q_H$ for all examples, the first term in (15) vanishes. The error is hence bounded by $k^{d/2} \lambda (H/h)^2 \theta^{k/\lambda(H/h)} \|f\|_{L^2(\Omega)}$, which allows for a careful investigation of the influence of k , H and h . A reference line proportional to H^2 is plotted for guidance. We can see that we achieve convergence for both choices of C . However, since k is rounded to an integer, the convergence plots have a staggered appearance. This example shows that the error due to localization can be kept small and decreases with H . The plots also show the relative error in energy norm for the standard Raviart–Thomas discretization on the coarse mesh. It is evident that the localized multiscale space has good approximation properties since it permits convergence while the standard space of the same dimension does not.

5.2 Investigation of instability

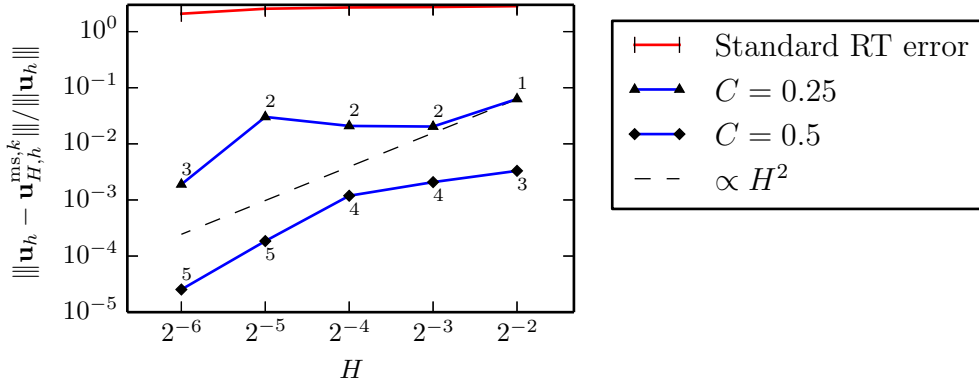
In this experiment we show how singularity-like features can appear in the solution, probably as a result of high contrast in combination with the L^2 -instability of the nodal Raviart–Thomas interpolator.

Again, we consider the unit square $\Omega = [0, 1]^2$. The diffusion coefficient A is chosen according to Figure 5. In other words, A is defined as

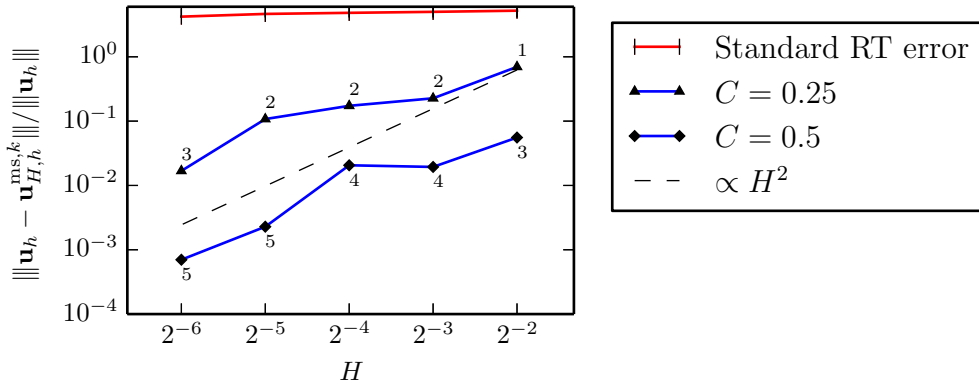
$$A(x) = \begin{cases} \exp(10) & \text{if } x_2 < 1/2 \text{ or } x \in [\frac{1}{2} - 2^{-5}, \frac{1}{2} + 2^{-5}] \times [\frac{1}{2}, \frac{1}{2} + 2^{-5}], \\ 1 & \text{otherwise.} \end{cases}$$



(a) Diffusion coefficient is constant.



(b) Diffusion coefficient is noisy.



(c) Diffusion coefficient has channel structures.

Figure 4: Convergence plots for localization error experiments. Relative error in energy norm for three choices of A , for different values of the constant C determining the patch size. The number adjacent to a point is the actual value of k for the specific simulation corresponding to that point.

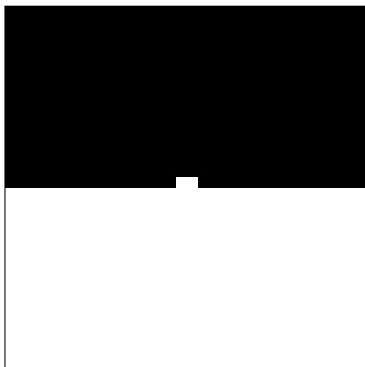


Figure 5: Coefficient A defined on a $2^5 \times 2^5$ grid of Ω where $A(x) = 1$ for x in black cells and $A(x) = \exp(10)$ for x in white cells.

The source function is chosen as

$$f(x) = \begin{cases} -1 & \text{if } x_2 < 1/2, \\ 1 & \text{otherwise.} \end{cases}$$

This particular choice of A and f yields a localized multiscale solution with a clear singularity-like feature at $x = (x_1, x_2) = (1/2, 1/2)$ in the localized multiscale solution.

We use the family of triangulations presented in Figure 3 and fix $H = 1/4$ so that f is resolved on the coarse scale. Then $f \in Q_H$ and all error stems from localization (see Theorem 16). We let the resolution h of the fine space be $h = 2^{-5}, 2^{-6}, \dots, 2^{-9}$. Choosing $k = 2$, we compute the localized multiscale solution $\mathbf{u}_{H,h}^{\text{ms},k}$ and reference solution \mathbf{u}_h for the given values of h .

From the error estimate in Theorem 16, we expect to have

$$\begin{aligned} \left\| \mathbf{u}_h - \mathbf{u}_{H,h}^{\text{ms},k} \right\| &\lesssim k^{d/2} \lambda (H/h)^2 \theta^{k/\lambda(H/h)} \|f\|_{L^2(\Omega)} \\ &\propto \log(h^{-1}) \quad \text{as } h \rightarrow 0. \end{aligned}$$

The energy norm of the error is plotted in Figure 6. We can see that for this particular problem and range of h , the error increases with h and with the rate $\log(h^{-1})$ as predicted by the error estimate. However, the error estimate seems not to be sharp for this particular example. Figure 7 shows the reference and multiscale flux solutions. The magnitude of the reference solution is in the range $[0, 3]$, while the multiscale solution has a spike reaching magnitude 30 at $x = (1/2, 1/2)$. Interesting to note is that the singularities vanish for the ideal multiscale method, i.e. without localization, see Lemma 9.

5.3 Convergence in an L-shaped domain

Next, we consider an L-shaped domain with noisy diffusion coefficient A (case 2. in Section 5.1) and with $f \notin Q_H$. In this experiment, we show that the localization error investigated in the previous section can be dominated by errors from projecting f .

We use the domain $\Omega = [0, 1]^2 \setminus [1/2, 1] \times [0, 1/2]$ and the triangulation presented in Figure 8. Both fine and coarse meshes are constructed as shown in the figure. Further,

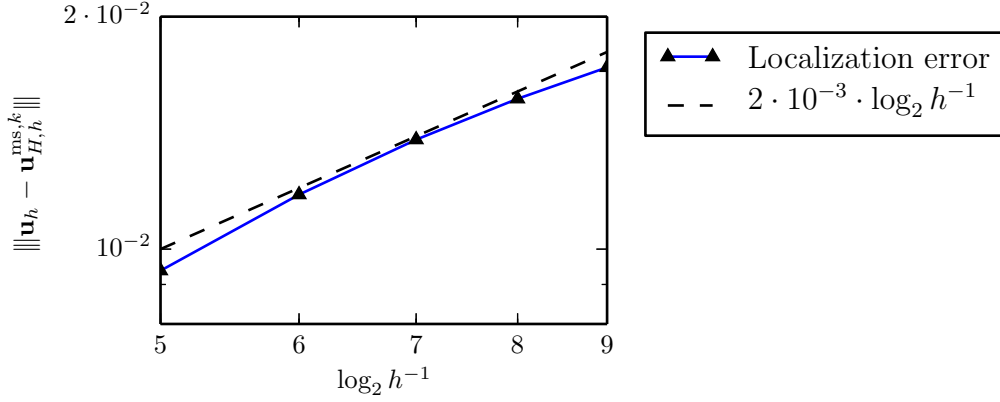


Figure 6: Divergence of the energy norm of the localization error of a particular multiscale solution as h decreases.

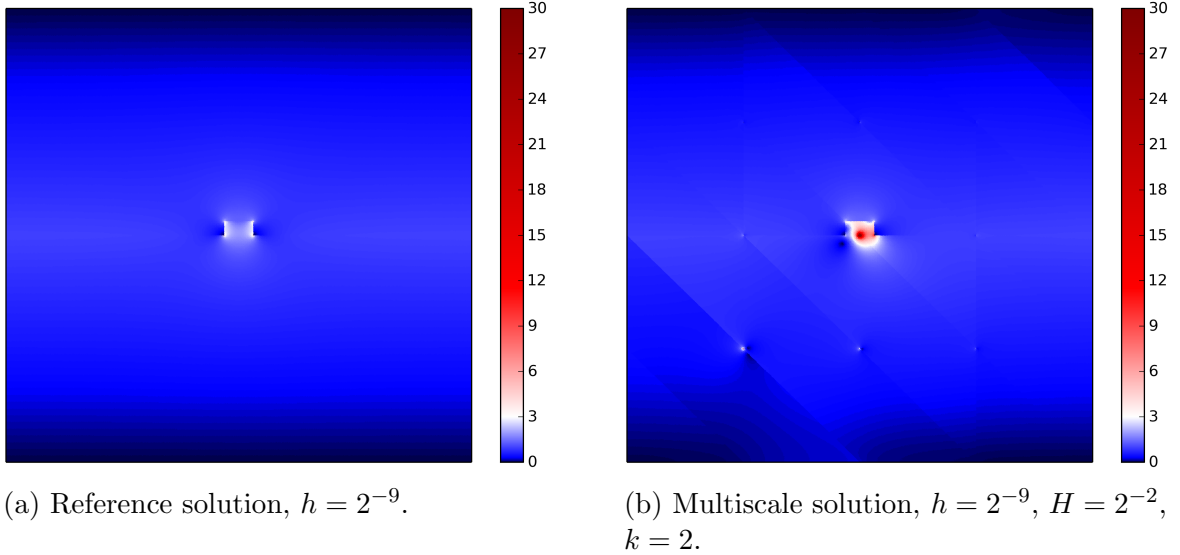


Figure 7: Magnitude of flux at the centroid of the triangles.

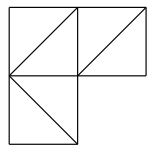
we choose the source function as

$$f(x) = \begin{cases} 1/2 + x_1 - x_2 & \text{if } x_2 < 1/2, \\ -(1/2 + x_1 - x_2) & \text{if } x_1 > 1/2, \\ 0 & \text{otherwise.} \end{cases}$$

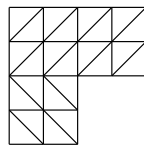
Note that $f \notin Q_H$ and $\|f - P_H f\|_{L^2(\Omega)} \lesssim H$. A reference solution \mathbf{u}_h was computed with the standard Raviart–Thomas spaces V_h and Q_h with $h = 2^{-8}$. Solutions $\mathbf{u}_{H,h}^{\text{ms},k}$ to the localized multiscale problem were computed using $H = 2^{-2}, 2^{-3}, \dots, 2^{-6}$. The patch size k was chosen as

$$k = C(1 + \log_2(H/h))^{1/2} \log_2(H^{-1})$$

rounded to the nearest integer, with $C = 0.25$ and $C = 0.5$. The relative error in energy norm was recorded for the solutions corresponding to the values of H . The resulting



(a) Coarsest mesh, $h = 1/2$.



(b) One refinement, $h = 1/4$.

Figure 8: Family of triangulations of the L-shaped domain.

convergence plot can be found in Figure 9. We expect the first term in the error estimate,

$$\left\| \mathbf{u}_h - \mathbf{u}_{H,h}^{\text{ms},k} \right\| \lesssim H \|f - P_H f\|_{L^2(\Omega)} + k^{d/2} \lambda(H/h) \theta^{k/\lambda(H/h)} \|f\|_{L^2(\Omega)} \quad (34)$$

to be of order H^2 . From the convergence plots we can see that $C = 0.25$ is not sufficient to make the localization error of at least order H^2 , however, $C = 0.5$.

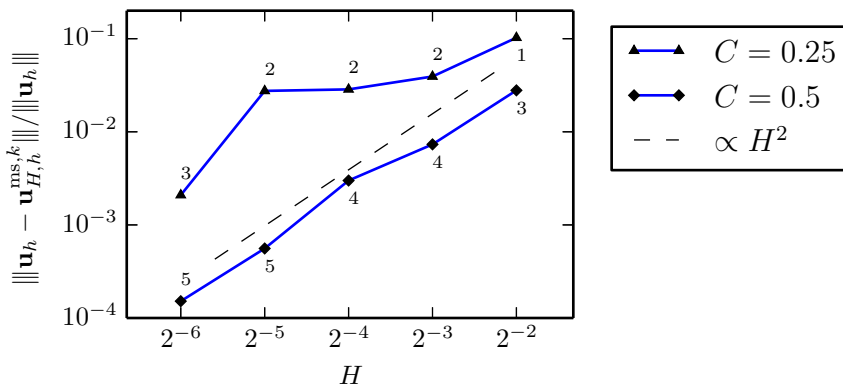


Figure 9: Convergence plot for experiment with L-shaped domain. Shows relative error in energy norm for two values of C and a series of values of H . The number adjacent to a point is the actual value of k for the specific simulation corresponding to that point.

5.4 Comparison with MsFEM

We compare the proposed method with the results obtained using the Multiscale Finite Element Method (MsFEM) based approach in [5]. The domain is $\Omega = [0, 1.2] \times [0, 2.2]$ and the permeability coefficient A is given in a uniform rectangular grid of size 60×220 by the 85th permeability layer in model 2 of SPE10 [12].

The method proposed in [5] is based on a fine and a coarse mesh with quadrilateral elements. The fine mesh is uniform 60×220 , i.e. aligned with the permeability data, and the coarse mesh is 6×22 , so that each coarse element is subdivided into 10×10 fine elements. The implementation of the method proposed in this work uses triangular meshes, which is why we divide each of the rectangular elements into two triangular elements by a diagonal line drawn from the upper left corner to the lower right corner. As coarse mesh, we use a similar triangular mesh that is constructed from a 6×22 rectangular mesh such that the fine mesh is a conforming refinement of the coarse mesh.

The (quasi-singular) source data f is equal to 1 in the lower left and -1 in the upper right fine quadrilateral element. Note that such f is a discretization of point sources

that model production wells. In particular, the source terms on the continuous level are mathematically described by Dirac delta functions. Hence, for $h \rightarrow 0$, we only have $f \in W^{-m,2}(\Omega)$ for $m > \frac{d}{2}$, opposed to $f \in L^2(\Omega)$ as is required for our analysis. To account for this difference, we follow [28] and compute the localized source corrections $F_h^{T,\ell} f \in V_h^f(U_\ell(T))$ on ℓ -coarse-layer patches for $T \in \mathcal{T}_H$,

$$a(F_h^{T,\ell} f, \mathbf{v}_h^f) + b(\mathbf{v}_h^f, \tilde{F}_h^{T,\ell} f) + b(F_h^{T,\ell} f, q_h^f) = -(f, q_h^f)_T,$$

for all $\mathbf{v}_h^f \in V_h^f(U_\ell(T))$ and $q_h^f \in Q_h^f(U_\ell(T))$, where $Q_h^f(U_\ell(T))$ is the restriction of Q_h^f to $U_\ell(T)$, analogous to the definition of $V_h^f(U_\ell(T))$. (The pressure solution $\tilde{F}_h^{T,\ell} f$ is not needed for correcting the flux and is discarded after its use as Lagrange multiplier). Since f is non-zero only for the two triangles T_1 and T_2 in the lower left and upper right corners, only two such corrector problems need to be solved. The total localized source correction is $F_h^\ell f = F_h^{T_1,\ell} f + F_h^{T_2,\ell} f \in V_h^f$.

The localized corrector problems (11) are unaffected by the source correction. The right hand side of the localized multiscale problem (12) is appended with the localized source corrections and instead reads: find $\mathbf{u}_{H,h}^{\text{ms},k,\ell}$ such that

$$a(\mathbf{u}_{H,h}^{\text{ms},k,\ell}, \mathbf{v}_h) + b(\mathbf{v}_h, p_H) + b(\mathbf{u}_{H,h}^{\text{ms},k,\ell}, q_H) = -(f, q_H) - a(F_h^\ell f, \mathbf{v}_h).$$

Using a value of $\ell = 0$ will be referred to as an ad-hoc source correction, since we do not expect to have any decay of the correction already within the source triangle itself. The source corrected solution is $\mathbf{u}_{H,h}^{\text{ms},k,\ell} + F_h^\ell f$.

We emphasize that the need for source correctors for singular source terms is not an exclusive drawback for our approach, but it is a common necessity shared by all comparable multiscale methods in this setting. In particular they are also used for the MsFEM-based approach in [5] that we use for our comparative study.

The proposed localized multiscale method was used to solve for the flux in the described problem for three corrector patch sizes: $k = 1, 2$, and 3 . Three variants of source correction were used: i) without source correction, i.e. $\mathbf{u}_{H,h}^{\text{ms},k}$, ii) with ad-hoc source correction, i.e. $\mathbf{u}_{H,h}^{\text{ms},k,\ell} + F_h^\ell f$ for $\ell = 0$ (without interpolation constraint), and iii) with source correction, i.e. $\mathbf{u}_{H,h}^{\text{ms},k,\ell} + F_h^\ell f$ for $\ell = k, k+1, \infty$. A reference solution \mathbf{u}_h was computed on the fine mesh. Table 1 shows the relative energy norm and L^2 -norm of the difference between the localized multiscale solution and the reference solution for the different values of k and ℓ . The corresponding L^2 -norm of the error for the MsFEM method with oversampling HE0-OS proposed in [5] is also presented in the table. Note that HE0-OS is based on a discretization with roughly 33% less degrees of freedom than the proposed method, since it uses quadrilaterals instead of triangles (however, since this holds for both the fine and the coarse mesh, the relative change in the amount of degrees of freedom with respect to the reference solution is the same). The flux solutions are plotted in Figure 10.

The results show that the proposed method even without error correction compares favorably with the homogenization based approach. Ad-hoc error correction gives small errors for this problem in both norms. For source correction with patch size $\ell = k$, instabilities similar to that studied in Section 5.2 cause the error to increase. However, letting $\ell = k+1$ is enough to get errors that compare favorably with [5].

Table 1: Relative error in energy norm and L^2 -norm for the SPE10-85 problem.

Method	k	ℓ	Energy norm	L^2 -norm
Proposed method without source correction	1	–	0.7863	0.4069
	2	–	0.7856	0.3369
	3	–	0.7855	0.3325
Proposed method with ad-hoc source correction ($\ell = 0$)	1	0	0.1541	0.2700
	2	0	0.1515	0.1467
	3	0	0.1537	0.1379
	1	1	0.1090	0.8292
	1	2	0.0459	0.2703
	1	∞	0.0350	0.2504
Proposed method with source correction ($\ell = k, k + 1, \infty$)	2	2	0.0549	0.7453
	2	3	0.0185	0.0517
	2	∞	0.0150	0.0490
	3	3	0.0080	0.0178
	3	4	0.0051	0.0424
	3	∞	0.0041	0.0088
HE0-OS [5]	–	–	–	0.3492

Acknowledgement

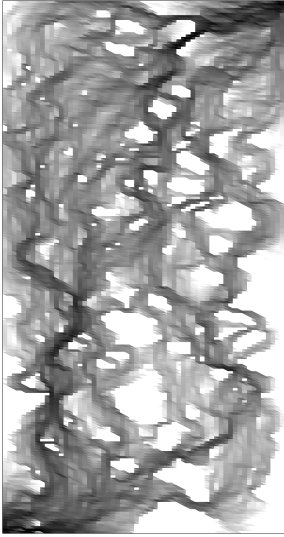
We gratefully acknowledge the anonymous reviewers for their careful reading and insightful suggestions that improved the manuscript.

References

- [1] J. Aarnes. On the use of a mixed multiscale finite element method for greater flexibility and increased speed or improved accuracy in reservoir simulation. *Multiscale Model. Simul.*, 2(3):421–439, 2004.
- [2] A. Abdulle and P. Henning. A reduced basis localized orthogonal decomposition. *J. Comput. Phys.*, 295:379–401, 2015.
- [3] A. Abdulle and P. Henning. Localized orthogonal decomposition method for the wave equation with a continuum of scales. *ArXiv e-print 1406.6325*, to appear in *Math. Comp.*, 2016+.
- [4] T. Arbogast. Analysis of a two-scale, locally conservative subgrid upscaling for elliptic problems. *SIAM J. Numer. Anal.*, 42(2):576–598 (electronic), 2004.
- [5] T. Arbogast. Homogenization-based mixed multiscale finite elements for problems with anisotropy. *Multiscale Model. Simul.*, 9(2):624–653, 2011.

- [6] T. Arbogast and K. Boyd. Subgrid upscaling and mixed multiscale finite elements. *SIAM J. Numer. Anal.*, 44(3):1150–1171, 2006.
- [7] D. N. Arnold, R. S. Falk, and R. Winther. Finite element exterior calculus, homological techniques, and applications. *Acta Numer.*, 15:1–155, 2006.
- [8] D. Boffi, F. Brezzi, and M. Fortin. *Mixed Finite Element Methods and Applications*, volume 44 of *Springer Series in Computational Mathematics*. Springer-Verlag, Berlin Heidelberg, 2nd edition, 2013.
- [9] Z. Chen and T. Y. Hou. A mixed multiscale finite element method for elliptic problems with oscillating coefficients. *Math. Comp.*, 72:541–576, 2003.
- [10] S. H. Christiansen. Stability of Hodge decompositions in finite element spaces of differential forms in arbitrary dimension. *Numer. Math.*, 107(1):87–106, 2007.
- [11] S. H. Christiansen and R. Winther. Smoothed projections in finite element exterior calculus. *Math. Comp.*, 77(262):813–829, 2008.
- [12] M. A. Christie. Tenth SPE comparative solution project: A comparison of upscaling techniques. *SPE Reservoir Eval. Eng.*, 4:308–317, 2001.
- [13] D. Elfverson, E. H. Georgoulis, A. Målqvist, and D. Peterseim. Convergence of a discontinuous Galerkin multiscale method. *SIAM J. Numer. Anal.*, 51(6):3351–3372, 2013.
- [14] D. Elfverson, V. Ginting, and P. Henning. On multiscale methods in Petrov-Galerkin formulation. *Numer. Math.*, 131(4):643–682, 2015.
- [15] P. Henning and A. Målqvist. Localized orthogonal decomposition techniques for boundary value problems. *SIAM J. Sci. Comput.*, 36(4):A1609–A1634, 2014.
- [16] P. Henning, A. Målqvist, and D. Peterseim. A localized orthogonal decomposition method for semi-linear elliptic problems. *ESAIM Math. Model. Numer. Anal.*, 48(5):1331–1349, 2014.
- [17] P. Henning, P. Morgenstern, and D. Peterseim. Multiscale partition of unity. In M. Griebel and M. A. Schweitzer, editors, *Meshfree Methods for Partial Differential Equations VII*, volume 100 of *Lecture Notes in Computational Science and Engineering*, pages 185–204. Springer International Publishing, 2015.
- [18] P. Henning and D. Peterseim. Oversampling for the multiscale finite element method. *Multiscale Model. Simul.*, 11(4):1149–1175, 2013.
- [19] T. Y. Hou and X.-H. Wu. A multiscale finite element method for elliptic problems in composite materials and porous media. *J. Comput. Phys.*, 134(1):169 – 189, 1997.
- [20] T. Hughes and G. Sangalli. Variational multiscale analysis: the fine-scale Green’s function, projection, optimization, localization, and stabilized methods. *SIAM J. Numer. Anal.*, 45(2):539–557, 2007.

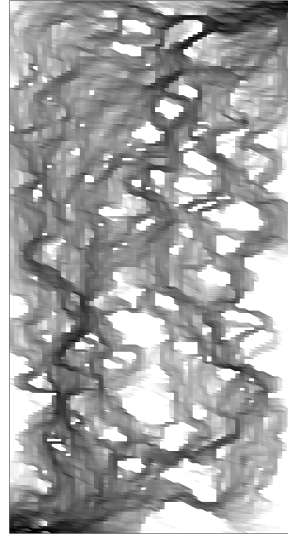
- [21] T. J. R. Hughes. Multiscale phenomena: Green’s functions, the Dirichlet-to-Neumann formulation, subgrid scale models, bubbles and the origins of stabilized methods. *Comput. Methods Appl. Mech. Engrg.*, 127(1-4):387–401, 1995.
- [22] T. J. R. Hughes, G. R. Feijóo, L. Mazzei, and J.-B. Quinicy. The variational multiscale method—a paradigm for computational mechanics. *Comput. Methods Appl. Mech. Engrg.*, 166(1-2):3–24, 1998.
- [23] D. Iftimie, G. Karch, and C. Lacave. Asymptotics of solutions to the Navier-Stokes system in exterior domains. *J. Lond. Math. Soc. (2)*, 90(3):785–806, 2014.
- [24] M. G. Larson and A. Målqvist. Adaptive variational multiscale methods based on a posteriori error estimation: Energy norm estimates for elliptic problems. *Comput. Methods Appl. Mech. Engrg.*, 196:2313–2324, 2007.
- [25] M. G. Larson and A. Målqvist. A mixed adaptive variational multiscale method with applications in oil reservoir simulation. *Math. Models Methods Appl. Sci.*, 19(07):1017–1042, 2009.
- [26] A. Målqvist and D. Peterseim. Localization of elliptic multiscale problems. *Math. Comp.*, 83(290):2583–2603, 2014.
- [27] A. Målqvist and D. Peterseim. Computation of eigenvalues by numerical upscaling. *Numer. Math.*, 130(2):337–361, 2015.
- [28] A. Målqvist. Multiscale methods for elliptic problems. *Multiscale Model. Simul.*, 9(3):1064–1086, 2011.
- [29] J. Nolen, G. Papanicolaou, and O. Pironneau. A framework for adaptive multiscale methods for elliptic problems. *Multiscale Model. Simul.*, 7(1):171–196, 2008.
- [30] D. Peterseim. Eliminating the pollution effect in Helmholtz problems by local sub-scale correction. *to appear in Math. Comp.*, 2016+.
- [31] P. A. Raviart and J. M. Thomas. A mixed finite element method for 2-nd order elliptic problems. In I. Galligani and E. Magenes, editors, *Mathematical Aspects of Finite Element Methods*, volume 606 of *Lecture Notes in Mathematics*, pages 292–315. Springer Berlin Heidelberg, 1977.
- [32] J. Schöberl. A posteriori error estimates for Maxwell equations. *Math. Comp.*, 77(262):633–649, 2008.
- [33] H. Wendland. Divergence-free kernel methods for approximating the Stokes problem. *SIAM J. Numer. Anal.*, 47(4):3158–3179, 2009.
- [34] B. Wohlmuth, A. Toselli, and O. Widlund. An iterative substructuring method for Raviart–Thomas vector fields in three dimensions. *SIAM J. Numer. Anal.*, 37(5):1657–1676, 2000.



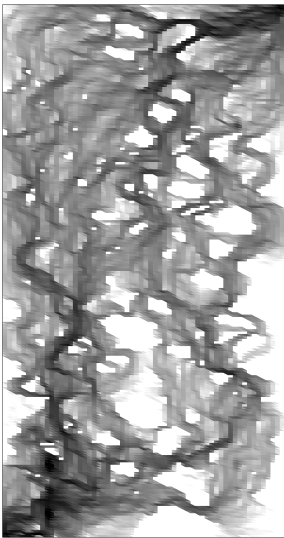
(a) Reference solution



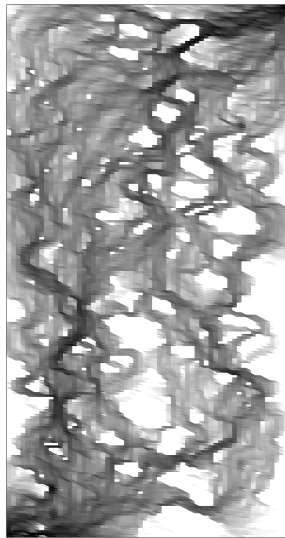
(b) $k = 1, \ell = -1$



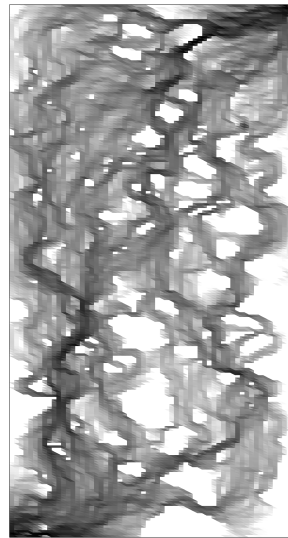
(c) $k = 1, \ell = 0$



(d) $k = 1, \ell = 1$



(e) $k = 1, \ell = 2$



(f) $k = 2, \ell = 3$

Figure 10: Flux solutions for the SPE10-85 problem. Figure (a) shows the reference flux solution and (b–f) show the multiscale flux solutions for $k = 1$ and 2 , and different source corrections ($\ell = -1$ means no source correction and $\ell = 0$ means ad-hoc error correction). The color maps to the magnitude of the flux at the midpoint of the triangular elements. The colors map from 10^{-5} (white) to 10^{-2} (black) and is saturated at white and black for lower and higher values, respectively.